Contributions to Mineralogy and Petrology (2021) 176:31
https://doi.org/10.1007/s00410-021-01787-4

ORIGINAL PAPER

Origin of the primitive, strongly SiO_2-undersaturated alkalic rocks from the Deccan Traps by low-degree mantle melting and high-pressure fractional crystallization

Nilanjan Chatterjee[1]

Received: 20 December 2019 / Accepted: 6 March 2021 / Published online: 3 April 2021

Abstract
Strongly SiO_2-undersaturated alkalic rocks (Mg# > 50, $SiO_2 \leq 45$ wt%, $Na_2O + K_2O \geq 3$ wt%) occur in three early-stage (Sarnu-Dandali, Mundwara, Bhuj) and one late-stage (Murud-Janjira) rift-associated volcanic complexes in the Cretaceous-Paleogene Deccan Traps flood basalt province of India. Thermobarometry based on clinopyroxene-liquid equilibrium suggests that they mostly crystallized beneath the Moho at ~ 15 kbar/1270 °C to ~ 11–12 kbar/1115–1156 °C pressures and temperatures. Primary magma compositions in equilibrium with lherzolite were estimated through reverse fractionation calculations by incrementally adding equilibrium phases to the rocks in olivine:clinopyroxene:spinel:phlogopite = 12:68:20:15 proportions at low temperatures followed by olivine:clinopyroxene:spinel = 12:68:20 proportions at higher temperatures. A comparison of the primary magmas with experimentally generated melts shows that their compositions are consistent with an origin from garnet lherzolite sources with < 1 wt% H_2O and CO_2. Hornblendite, pyroxenite (except for some Bhuj rocks) and carbonated eclogite are unlikely sources for the Deccan alkalic rocks. The Sarnu-Dandali and Bhuj alkalic rocks and the Murud-Janjira lamprophyres probably originated by < 5% melting of ~ 1.3 times Ti-enriched lherzolitic sources compared to primitive mantle. The primary magmas of the Murud-Janjira basanites calculated through reverse assimilation-fractional crystallization by assimilating lower crustal and mantle xenoliths found in younger lamprophyre dikes of the same area indicate that contamination by the Indian lithosphere was unlikely during their ascent. The basanites evolved by mixing with phonotephritic melts, and they probably originated from a Ti-poor (0.7 times) lherzolite source. The temperature of the melts at the base of the lithosphere was ~ 1325 °C beneath Sarnu-Dandali and ~ 1285 °C beneath Bhuj and Murud-Janjira.

Keywords Deccan Traps · SiO_2-undersaturated alkalic rock · Primary magma · Fractional crystallization · Lherzolite · Pyroxenite

Introduction

Continental flood basalt provinces are largely composed of tholeiites that originate by voluminous melting of the mantle as plumes ascend through upper mantle and encounter temperatures above the solidus (Morgan 1972; McKenzie and Bickle 1988; Richards et al. 1989; Campbell and Griffith 1990). By contrast, small amounts of alkalic volcanic rocks (e.g. nephelinite, basanite, tephrite, phonolite, trachybasalt, trachyte, etc.) present in flood basalt provinces are the products of low-degree mantle melting (Gast 1968; Green 1973). Determining the mantle source characteristics, degree of melting, and the pressure–temperature (P–T) conditions for the origin of alkalic rocks is an active area of petrological research. According to some experimental studies, the source is deep (~ 2.5–3.0 GPa) garnet lherzolite ± H_2O ± CO_2 (Dasgupta et al. 2007, 2013; Baasner et al. 2016; Condamine et al. 2016), whereas other experiments suggest a relatively shallow (~ 1.5 GPa) metasomatized lithospheric mantle as the likely source (Pilet et al. 2008, 2010). In addition, experiments have been conducted on garnet pyroxenite (Kogiso et al. 2003; Hirschmann et al. 2003) and eclogite ± CO_2 believed to be recycled into the mantle (Pertermann et al. 2004; Dasgupta et al. 2006) to

Communicated by Othmar Müntener.

✉ Nilanjan Chatterjee
nchat@mit.edu

[1] Department of Earth, Atmospheric and Planetary Sciences, Massachusetts Institute of Technology, Cambridge, MA 02139, USA

assess whether these lithologies can be the potential sources of alkalic rocks. This study attempts to determine the origin of primitive (molar 100.Mg/(Mg + Fe^{2+}), or Mg# > 51), strongly SiO_2-undersaturated alkalic rocks (SiO_2 = 36–45 wt %, $Na_2O + K_2O$ = 3–6 wt%, all oxides recalculated on a volatile-free basis) from the Deccan Traps of India by comparing the compositions of their bulk rock and calculated primary magmas (Mg# 72, in equilibrium with Fo_{90} olivine) with melts produced in high-pressure experiments.

Although some rare Deccan picrites from Saurashtra (Fig. 1) containing Fo_{88-92} olivine may be the progenitors of the locally associated tholeiitic basalts (Krishnamurthy and Cox 1977; Melluso et al. 1995), low-pressure reverse fractional crystallization modeling shows that the primary magmas of most Deccan tholeiites are primitive tholeiites that last equilibrated with lherzolitic mantle near the crust–mantle boundary (Chatterjee and Sheth 2015, using the methods of Till et al. 2012). A similar reverse fractionation approach is adopted here to calculate the primary magmas of the Deccan alkalic rocks. However, the Deccan tholeiites differentiated by fractionating gabbroic assemblages at low pressures (< 0.2 GPa, Bhattacharji et al. 1996; Sano et al. 2001), whereas thermobarometry in this study suggests that the Deccan alkalic rocks differentiated at much higher pressures (> 1.2 GPa). Hence, the appropriate assemblages and phase proportions that crystallize at high pressures from primitive alkalic melts (as in the experiments of Holbig and Grove 2008; Pilet et al. 2010) are recombined with the Deccan alkalic rocks to model their primary magmas. At the end of each calculation, the melt (Mg# 72) is in equilibrium with lherzolite containing Fo_{90} olivine. The mantle melting conditions for the origin of the Deccan alkalic rocks constrained by lherzolite melting experiments and geophysical data are discussed.

Geological background

The Deccan Traps of central and western India constitute one of the largest (≥ 500,000 km^2) continental flood basalt provinces on Earth with thick, near-horizontal tholeiitic lava sequences and rift-related minor alkalic rocks (Wadia 1975; Fig. 1). The bulk of the tholeiitic basalts at Western Ghats (Beane et al. 1986; Lightfoot et al. 1990) was erupted within a ~ 1 million year interval that straddles the Cretaceous-Paleogene boundary (66.4–65.4 Ma, Schoene et al., 2019; Sprain et al., 2019). By contrast, the alkalic rocks associated with the NNW–SSE oriented Barmer-Cambay Rift (68.6–68.5 Ma old Sarnu-Dandali and Mundwara complexes, Chandrasekaran et al. 1990; Basu et al. 1993) and the E–W-oriented Kachchh Rift (67.0–66.8 Ma old Bhuj alkalic plugs, Krishnamurthy et al. 1999; Courtillot et al. 2000) in the northwestern part were emplaced before, and the alkalic rocks at the rifted western continental margin

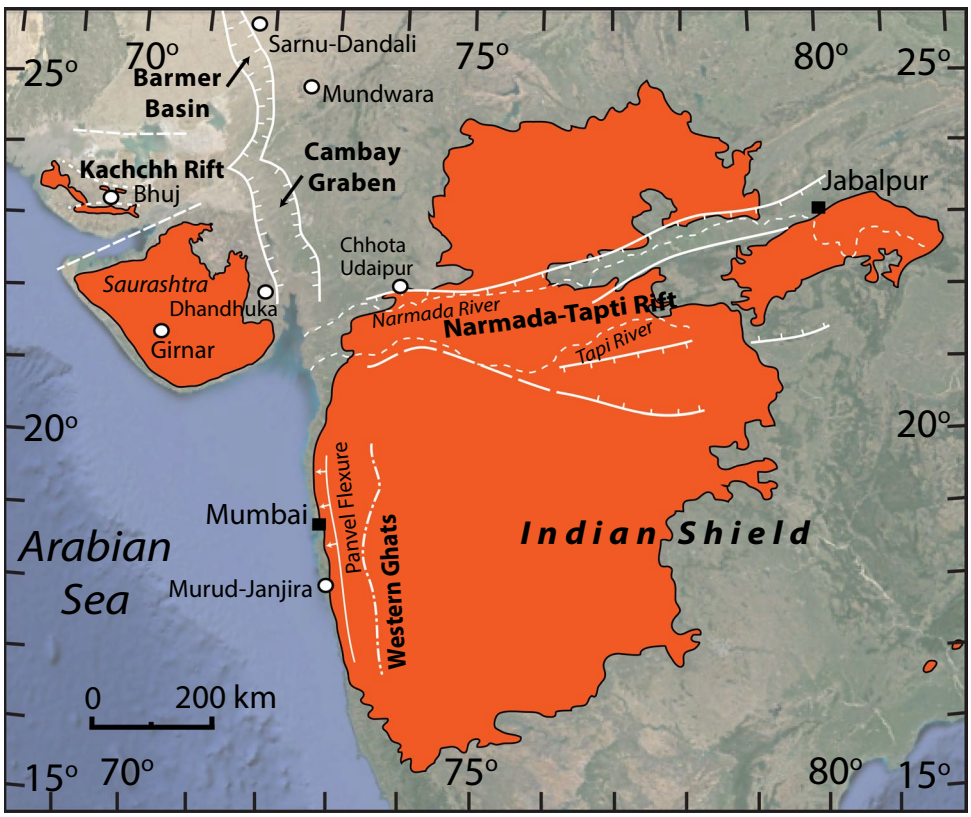

Fig. 1 Google satellite image of the Indian Shield region overlain by a map showing the areal extent of Deccan Traps with rift zones, faults, location of alkalic complexes, and important places

(Murud-Janjira plugs and dikes, Dessai et al. 1990) were emplaced after the Western Ghats tholeiites. It is worth noting that the Sarnu-Dandali and Mundwara complexes have protracted magmatic histories and also contain older alkalic rocks unrelated to Deccan (c. 110–80 Ma, Pande et al. 2017; Sheth et al. 2017).

The Deccan flood basalt province probably formed when the northward drifting Indian plate was over a mantle hot spot (Deccan plume) (Devey and Lightfoot 1986; Mitchell and Widdowson 1991). Extreme upwarping of the Moho (~ 18 km depth) and lithospheric thinning (~ 40 km depth) are evident at the rifted western Indian continental margin including the Murud-Janjira area located ~ 300 km south of the postulated Deccan plume center (Negi et al. 1992; Bhattacharji et al. 1996 and references therein). Thinned crust (Cambay: 28–35 km, Kachchh: 29–43 km) and lithosphere (Cambay: 85–90 km, Kachchh: 63–69 km) within the rift zones of the northwestern Deccan province close to the northern periphery of the Deccan plume (at a distance of ~ 400–530 km from the center) have been also attributed to mantle upwelling (Rao et al. 2015; Radha Krishna et al. 2002; Mandal and Pandey 2011).

Strongly SiO_2-undersaturated Deccan alkalic rocks

The Sarnu-Dandali and Mundwara primitive alkalic rocks show Reunion plume-type high $^{3}He/^{4}He$ ratios (Basu et al. 1993). Their range of initial $^{143}Nd/^{144}Nd$ ratios is 0.5127–0.5128 (Simonetti et al. 1998). In an Sr–Nd isotope plot, the Sarnu-Dandali primitive rocks (initial $^{87}Sr/^{86}Sr$: 0.7043–0.7045, Basu et al. 1993; Simonetti et al. 1998) plot near the depleted end (close to Reunion lavas) of a mixing array between Reunion-type mantle and continental lithosphere indicating that their source was not significantly influenced by the continental lithosphere. However, the higher initial $^{87}Sr/^{86}Sr$ ratios of the Mundwara samples considered in this study (0.7045–0.7048, Basu et al. 1993; Simonetti et al. 1998) indicate that their source formed by mixing of a Reunion-type mantle with a lithospheric component.

The Sarnu-Dandali alkalic rocks occur as lava flows, and plugs and dikes intruding older plutons (Chandrasekaran et al. 1990; Sheth et al. 2017). In a total alkali versus silica (TAS) diagram (Le Bas et al. 1986), most of the primitive samples (Chandrasekaran et al. 1990; Simonetti et al. 1998; Vijayan et al. 2016) plot in the foidite field (Fig. 2a), the evolved samples plot in the phonolite field, and a few other samples plot in the tephrite/basanite, trachyandesite and trachyte fields (not shown). They show high Ce/Y ratios compared to the common Deccan tholeiites (Wai Subgroup, Fig. 2f), a feature consistent with origin from a garnet-bearing mantle source. The Ni and Cr contents are positively correlated with MgO (Fig. 2g, h). The lowest-SiO_2 rocks with < 6.2 wt% $Na_2O + K_2O$ (K_2O = 1.4–2.6 wt%, Na_2O/K_2O = 1.2–2.1) are also the most primitive (SiO_2 = 36.3–39.6 wt%, MgO = 8.2–11.5 wt%, Mg# 52–65, Fig. 2c, Table 1). These rare rocks are variously reported as melanephelinite (Vijayan et al. 2016), alkali pyroxenite, micro-melteigite (Chandrasekaran et al. 1990) and melilitite with fine-grained microporphyritic textures (Simonetti et al. 1998). Their TiO_2 (3.5–6.4 wt%) and CaO (13.8–18.1 wt%) contents, and CaO/Al_2O_3 ratios (1.3–1.6) are the highest among all Deccan rocks. They also contain 1.0–2.5 wt% H_2O and ~ 0.4 wt% CO_2, determined by gravimetric methods (Chandrasekaran et al. 1990). Carbonatites are commonly associated with the Sarnu-Dandali alkalic rocks (Chandrasekaran et al. 1990).

The Mundwara alkalic rocks occur as dikes intruding three distinct plutons (Pande et al. 2017 and references therein). According to the TAS classification, they mostly belong to the tephrite/basanite-phonolite series (Fig. 2a), and a few are basalts and trachybasalts (Simonetti et al. 1998; Pande et al. 2017). The most primitive rocks contain 7.3–8.4 wt% MgO (Mg# 51–58) and 41.4–44.2 wt% SiO_2 (Table 1). They have higher SiO_2, but similar total alkali, K_2O, TiO_2, Ce/Y, Ni and Cr values compared to the Sarnu-Dandali rocks (Fig. 2). Their REE contents are consistent with 0.5–2.0% melting of a garnet peridotite source (Basu et al. 1993).

The Bhuj primitive alkalic rocks, some of which contain spinel lherzolite xenoliths, occur as plug-like bodies belonging to a monogenetic volcanic field in the central part of the Kachchh Rift (Kshirsagar et al. 2011 and references therein). In the TAS diagram, most of the primitive samples (Simonetti et al. 1998; Karmalkar et al. 2005; Kshirsagar et al. 2011) plot in the tephrite/basanite field, and a few plot in the foidite field (Fig. 2a). Other samples (Paul et al. 2008; Sen et al. 2009) plot in the basalt and trachybasalt fields (not shown). The samples from Simonetti et al. (1998) have similar initial $^{87}Sr/^{86}Sr$ (0.7036–0.7040) and $^{143}Nd/^{144}Nd$ (0.5128–0.5129) ratios to the Reunion and enriched Central Indian Ridge (CIR) basalts, indicating an absence of lithospheric contamination. The primitive samples are composed of fine- to medium-grained, feebly porphyritic lava with 10–20% phenocryst content (Simonetti et al. 1998; Krishnamurthy et al. 1999). They contain 9.3–15.9 wt% MgO (Mg# 57–72). Compared to the Sarnu-Dandali primitive rocks, the Bhuj primitive rocks contain higher SiO_2 (39.6–45.2 wt%), similar K_2O (0.7–2.5 wt%), and lower TiO_2 (2.6–3.8 wt%), CaO (10.0–12.3 wt%), CaO/Al_2O_3 and Ce/Y (Fig. 2a-f, Table 1). They cover a broader range of Na_2O/K_2O ratios (1.0–4.8) than the Sarnu-Dandali rocks, and their range of Ba/Nb ratios is 8–18. They contain 1.3–3.3 wt% H_2O and 0.07–0.24 wt% CO_2 determined by gravimetric methods (Karmalkar et al. 2005). They also contain high Ni (168–464 ppm) and Cr (334–995 pm) that are positively correlated with MgO (Fig. 2g,h) (Simonetti

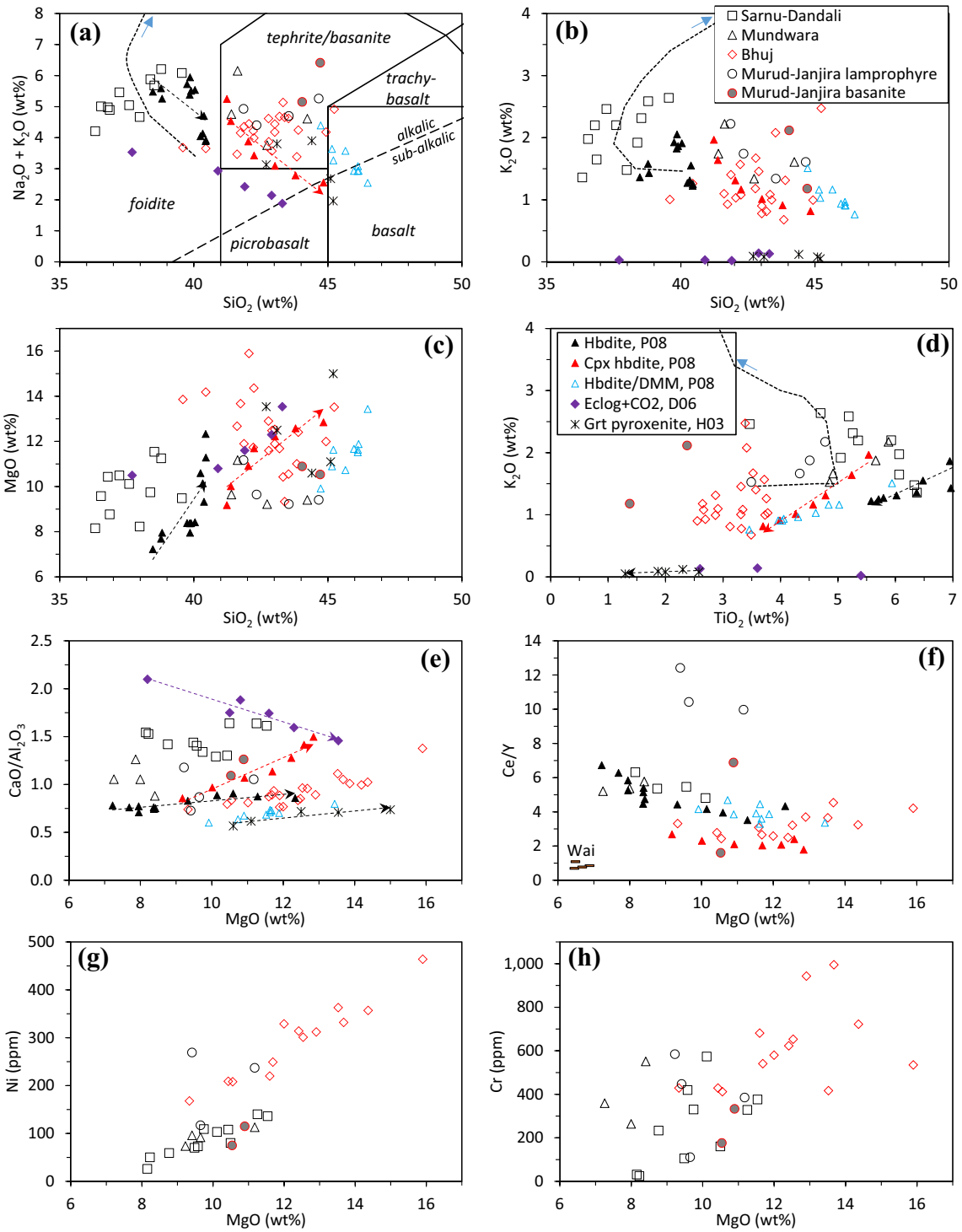

Fig. 2 Bulk compositions of the Deccan primitive alkalic rocks recalculated on a volatile-free basis and experimentally derived melts (refer to legends in **b** and **d**); data sources as in text for the alkalic rocks, Beane et al. (1986) and Lightfoot et al. (1990) for the average Ce/Y ratios of Wai Subgroup basalts, and the experiments of D06: Dasgupta et al. (2006), H03: Hirschmann et al. (2003) and P08: Pilet et al. (2008). In **a**, the boundaries between different rock-types are from Le Bas et al. (1986) and the subalkalic-alkalic boundary is from Macdonald and Katsura (1964). The dotted lines in (**a**, **b** and **d**) represent model trends for the evolution of strongly SiO_2-undersaturated Cape Verde lavas (Weidendorfer et al. 2016). The melting trends for hornblendite, Cpx-hornblendite, eclogite + CO_2, and garnet pyroxenite are shown by dashed lines with arrows. *Hbdite* hornblendite, *Hbdite/DMM* hornblendite in equilibrium with depleted MORB mantle, *Eclog* eclogite

Table 1 Summary of bulk compositions of the primitive, strongly SiO_2-undersaturated alkalic rocks from the Deccan Traps

	SiO_2	TiO_2	Al_2O_3	FeO^T	MgO	CaO	K_2O	CaO/Al_2O_3	Na_2O+K_2O	Mg#
Sarnu-Dandali	36.3–39.6	3.46–6.38	9.2–11.2	12.0–15.9	8.2–11.5	13.8–18.1	1.36–2.64	1.29–1.64	4.21–6.21	51.7–64.9
Mundwara	41.4–44.2	4.85–5.88	10.7–12.8	12.5–15.5	7.3–8.4	11.2–13.6	1.34–2.22	0.88–1.26	3.76–6.15	51.0–57.9
Bhuj	39.6–45.2	2.55–3.78	8.3–13.7	11.5–14.9	9.3–15.9	10.0–12.3	0.68–2.47	0.74–1.38	3.39–5.13	57.4–71.9
Murud-Janjira										
Lamprophyre	41.9–44.7	3.49–4.78	10.3–12.7	14.2–15.7	9.2–11.2	9.2–12.1	1.53–2.18	0.73–1.18	4.40–5.26	55.7–60.3
Basanite	44.0–44.7	1.38–2.38	10.8–12.4	10.2–11.8	10.5–10.9	13.6–13.6	1.18–2.12	1.09–1.64	4.21–6.41	65.4–68.0

Data (oxide weight percentages recalculated on a volatile-free basis, FeO^T: total Fe expressed as FeO) from Chandrasekaran et al. (1990), Simonetti et al. (1998), Vijayan et al. (2016), Pande et al. (2017), Karmalkar et al. (2005), Paul et al. (2008), Kshirsagar et al. (2011), Dessai and Viegas (2010)

et al. 1998; Sen et al. 2009). Except for some diorites from Girnar (Bose, 1973), no other Deccan alkalic rocks have such high Ni contents. Incompatible element patterns of the Bhuj alkalic rocks generally resemble ocean island basalts (Sen et al. 2009), and their REE ratios indicate an origin by 2–6% melting of garnet peridotite (Karmalkar et al. 2005).

The Murud-Janjira lamprophyres, which also contain lower crustal and upper-mantle xenoliths derived from the Indian continental lithosphere, occur as N–S-oriented dikes cross-cutting older tholeiitic dikes and flows about 50–80 km south of Mumbai along the coast (Dessai et al. 1990, 2004; Melluso et al. 2002 and references therein). Four of the nine lamprophyre samples from Dessai and Viegas (2010) have primitive compositions (SiO_2 = 41.9–44.7 wt%, MgO = 9.2–12.1 wt%, Mg# 56–60, Table 1). They contain 3.5–4.8 wt % TiO_2 and 1.5–2.2 wt% K_2O (Na_2O/K_2O = 1.0–2.4), and show LILE enrichment (Ba/Nb = 4–11), high Zr (164–475 ppm) and Nb (39–209 ppm) contents with low Zr/Nb ratios (~ 2–4), and very high Ce/Y ratios indicating a garnet-bearing source (Fig. 2f). The range of Ni and Cr contents is 117–269 ppm and 111–584 ppm, respectively (Fig. 2g, h), though the Cr content of a basaltic lamprophyre is as high as 991 ppm (not shown). Based on their high Zr and Nb contents, Melluso et al. (2002) suggested low degrees (2–3%) of non-modal fractional melting of an enriched mantle source for the origin of the lamprophyres.

The Murud-Janjira nepheline-rich rocks are younger than the tholeiites and older than the lamprophyres. They occur in an E–W-oriented plug that cross-cuts the older tholeiitic dikes, and N–S-oriented dike or stock-like intrusions at the coast (Dessai and Viegas 2010; Melluso et al. 2002 and references therein). Two of the three samples from the plug (RG3 and RG1, Dessai et al. 1990; Dessai and Viegas 2010) are primitive basanites (Mg# 65–68) that contain 1.4–2.4 wt% TiO_2 and 3.0–5.2 wt% Na_2O (Na_2O/K_2O = 1.4–4.4) with highly enriched LILE patterns and variable Ce/Y ratios (Table 1, Fig. 2). Their Zr/Nb ratios are similar to the lamprophyres, but their Ba/Nb ratios (16–37) are much higher and they contain much lower Zr (59–195 ppm), Nb (13–68 ppm), La, Ce and Y. The third sample from the plug (RG2, Dessai et al. 1990) is a phonotephrite. Thin veins of carbonatite occur within the plug. The stock-like intrusion consists of melanephelinite, nephelinite and tephriphonolite (Dessai et al. 1990; Melluso et al. 2002). The melanephelinites and nephelinites show low initial $^{87}Sr/^{86}Sr$ (0.7045–0.7049) as well as low initial $^{143}Nd/^{144}Nd$ (0.5117–0.5119) ratios indicating mixing between primitive mantle and a low $^{143}Nd/^{144}Nd$ contaminant that may have been derived from delaminated continental mantle or "Lewisian-type" lower crust (Melluso et al. 2002).

Table 2 Compositions of minerals and groundmass in the Sarnu melanephelinite sample SD11

	SiO_2	TiO_2	Al_2O_3	Cr_2O_3	FeO^T	MnO	MgO	CaO	Na_2O	K_2O	NiO	ZnO[a]	F
Phenocrysts													
Cpx(c)	51.28	1.22	4.94	0.08	5.16	0.06	15.93	21.35	0.79	0.00			
Cpx(oc)	48.17	2.08	6.37	0.11	6.26	0.07	14.21	22.27	0.67	0.01			
Cpx(r)	44.98	3.90	7.78	0.04	6.62	0.06	12.91	23.15	0.44	0.04			
Cpx(avg)	48.06	2.45	6.40	0.07	6.02	0.06	14.32	22.28	0.63	0.02			
Ol(c)	39.29	0.02	0.05		15.55	0.20	45.26	0.15			0.18		
Ol(oc)	38.90	0.03	0.05		17.79	0.24	43.28	0.27			0.07		
Ol(r)	39.28	0.05	0.04		17.37	0.29	43.66	0.39			0.03		
Ol(avg)	39.17	0.03	0.05		16.87	0.24	44.09	0.27			0.09		
Spl(c)	0.06	3.53	24.24	26.82	32.50	0.29	12.62	0.00			0.19	0.13	
Spl(r)	0.07	14.41	8.11	7.50	59.92	0.65	8.09	0.02			0.10	0.26	
Bt(pseud)	35.26	1.74	13.79	0.06	16.28	0.29	17.23	1.05	0.73	5.60	0.15	*0.11*	0.08
Inclusions													
Spl(Cpx-c)	1.43	4.45	12.86	2.45	66.50	0.57	5.68	0.93			0.16	0.10	
Spl(Cpx-r)	0.05	16.15	6.42	0.24	62.19	0.54	9.59	0.57			0.09	0.07	
Groundmass													
Bt	38.92	0.72	13.52	0.08	16.41	0.48	16.21	0.11	0.07	9.16	0.15	*0.02*	0.10
Fphl	33.39	5.86	13.65	0.03	6.89	0.09	18.01	0.07	0.25	6.25		*8.88*	5.07
Nph	41.71	0.02	33.58	0.00	1.09	0.00	0.14	0.36	15.75	6.77		*0.08*	0.04
GM[b]	38.58	3.89	15.35	0.04	9.52	0.10	7.44	12.58	6.22	1.90	0.02	*0.19*	0.13
Bulk[c]	36.79	5.35	10.98	0.00	15.94	0.18	10.43	14.29	2.78	2.20	0.01	*0.10*	

Ol olivine, *Cpx* clinopyroxene, *Spl* spinel, *Bt* biotite, *Fphl* fluorphlogopite, *Nph* nepheline, *c* core, *oc* outer core/mantle, *r* rim, *avg* average, *pseud* pseudomorph

Values in weight percent (atomic proportions and endmembers in Tables S1-S3)

[a]Instead of ZnO, BaO values are reported for Bt, Fphl, Nph, GM (groundmass) and Bulk

[b]Contains $P_2O_5 = 0.96$, $SO_3 = 0.05$ and $H_2O = 4.36$

[c]From Vijayan et al. (2016), recalculated on anydrous basis, contains FeO = 2.86, $Fe_2O_3 = 13.37$ (with oxybarometer, Blundy et al. 2020), $P_2O_5 = 0.77$, and H_2O from LOI = 2.23

Petrography and mineral chemistry

Mineral and groundmass compositions were analyzed on a JEOL JXA-8200 Superprobe electron probe microanalyzer (EPMA) at the Massachusetts Institute of Technology, Cambridge, MA, USA. Back-scattered electron (BSE) images and elemental X-ray maps were acquired with the same instrument. The EPMA was operated using an accelerating voltage of 15 kV and a beam current of 10 nA, and the raw data were corrected for matrix effects using the CIT-ZAF package (Armstrong 1995). The compositions of the phases and groundmass are listed in Table 2 and the Online Resource Supplementary Tables S1–S3.

The Sarnu melanephelinite sample SD11 has a porphyritic texture with large phenocrysts dominated by clinopyroxene (Cpx), and subordinate olivine (Ol), biotite (Bt) pseudomorphs, and spinel (Spl) (Fig. 3). Approximately, 50% by volume of the rock is composed of a fine-grained groundmass. Clinopyroxene is strongly zoned and shows distinct inner core (avg. $En_{47}Fs_9Wo_{45}$), outer core/mantle (avg. $En_{42}Fs_{10}Wo_{47}$) and rim (avg. $En_{39}Fs_{11}Wo_{50}$) domains with core-to-rim oscillatory trends of decreasing MgO and Na_2O and increasing Al_2O_3 and TiO_2 (Figs. 4a, 5). The jadeite content (< 5%) decreases from core to rim (Fig. 5d). Olivine is also zoned with a high-Mg inner core (avg. Fo_{84}) and a lower-Mg outer core (avg. Fo_{81}) and rim (Fig. 4b, 6a). The NiO content decreases, and the MnO and CaO contents increase from core to rim (Fig. 6b). The spinel phenocrysts consist of a Cr–Al-rich core and a Fe–Ti-rich rim (Figs. 4c, 6c). Spinel also occurs as inclusions in clinopyroxene and olivine. The biotite pseudomorphs are recrystallized to the groundmass phases (Fig. 4d) and show a Mg-rich average composition ($Mg/(Mg + Fe^T) = 0.65$, where Fe^T is total Fe). The groundmass contains nepheline, fluorphlogopite, biotite and Fe-Ti oxides. Nepheline (15.8 wt% Na_2O, 6.8 wt% K_2O) is partially altered to natrolite. Fluorphlogopite ($Mg/(Mg + Fe^T) = 0.88$ to 0.82) is rich in BaO (3.0–8.9 wt%), TiO_2 (4.3–5.9 wt%) and F (5.6–5.1 wt%) and shows Ba and Ti incorporation by coupled substitutions (Fig. 6d, e) (cf. Tischendorf et al. 2007). Neither the groundmass biotite ($Mg/(Mg + Fe^T) = 0.64$) nor the biotite pseudomorphs contain significant Ba, Ti and F.

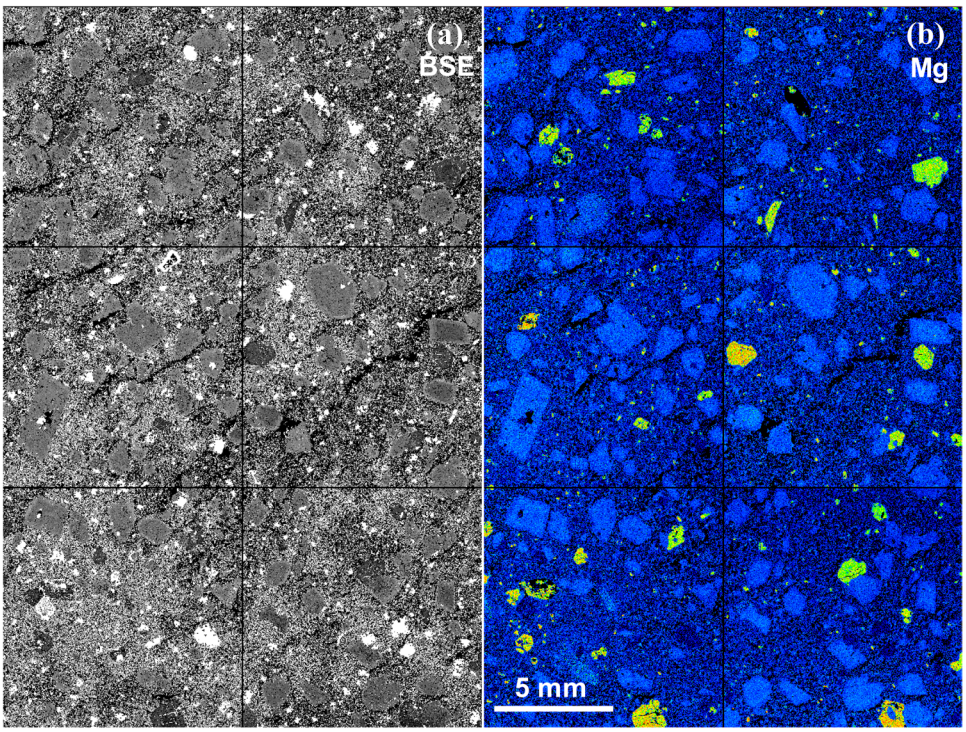

Fig. 3 **a** BSE image and **b** Mg x-ray map of Sarnu melanephelinite SD11 showing a porphyritic texture with large phenocrysts surrounded by a fine-grained groundmass. In (**a**), the bright grains are spinel and Fe-Ti oxides. In (**b**), the yellow-green Mg-rich crystals are olivine, and the euhedral, light-blue Mg-poor crystals are clinopyroxene. The images have a resolution of 10 micron, and were acquired using a stage-raster mode with a stationary beam

Thermobarometry

Thermobarometry was carried out using the clinopyroxene-liquid equilibrium formulations of Putirka (2008) with the bulk composition from Vijayan et al. (2016) (Table 3). Equilibrium was assessed on the basis of the mineral-bulk $K_D(Fe^{2+}–Mg)$ exchange coefficient with bulk Fe^{2+} estimated from the bulk $Fe^{3+}/\sum Fe$ ratio using the Fe–Mn–Mg exchange olivine-melt oxybarometer of Blundy et al. (2020). Since the oxybarometer formulation requires an equilibrium temperature, an initial temperature estimate was obtained by considering all Fe as Fe^{2+} and using the jadeite-diopside/hedenbergite (Jd-DiHd) formulations for Cpx-hydrous liquid equilibrium [Eqs. 30 and 33 of Putirka (2008), uncertainties: ± 3.6 kbar and ± 45 °C from regression analysis of experimental data] with loss-on-ignition as the H_2O content of the bulk. The Cpx-bulk $K_D(Fe^T–Mg)$ for the average and the outer core of Cpx are 0.28 and 0.29, and the estimated P–T are 14.9 kbar/1266 °C (average Cpx) and 15.5 kbar/1272 °C (Cpx outer core) (Table 3, S1). At 1270 °C, the lattice strain model (Blundy et al. 2020) predicts an equilibrium K_D(Mn–Mg) of 0.25 for the outer core of olivine that is within the uncertainty of the observed value (0.32 ± 0.08, based on uncertainties in Mn measurements with XRF and EPMA). Hence, the olivine outer core ($Fo_{81,}$ olivine-bulk $K_D(Fe^T–Mg) = 0.27$) was used to calculate the $Fe^{3+}/\sum Fe$ ratio of the bulk. The bulk $Fe^{3+}/\sum Fe$ ratio is 0.16, and the corresponding olivine-bulk $K_D(Fe^{2+}–Mg)$ of 0.32 is within the uncertainty of the equilibrium value (0.30 ± 0.03, Roeder and Emslie 1970). Considering a bulk $Fe^{3+}/\sum Fe$ ratio of 0.16, the $K_D(Fe^{2+}$-Mg) values for average Cpx-bulk (0.33) and Cpx outer core bulk (0.34) are within the uncertainty of the equilibrium Cpx-liquid $K_D(Fe^{2+}–Mg)$ value (0.28 ± 0.08, or 0.295 calculated with Eq. 35, Putirka, 2008). Hence, the P–T results calculated above are valid for Cpx-liquid equilibrium.

Equation 30 of Putirka (2008) is based on a selected, high-quality experimental data set. When Eq. 31 (Putirka 2008, uncertainty: ± 2.9 kbar) based on a global experimental data set is used, the estimated pressures are lower (12.2 kbar/1250 °C–12.6 kbar/1255 °C) but within the ± 3.6 kbar uncertainty for Eq. 30 (Table 3). On the other hand, when the Jd-DiHd formulations for the Cpx-anhydrous liquid exchange (Putirka et al. 1996) are used, the pressures are higher (17.0–17.6 kbar) but also within the ± 3.6 kbar uncertainty of the pressures calculated with the Cpx-hydrous liquid exchange equilibrium. Furthermore, the Al-exchange formulation between Cpx and hydrous liquid [Eq. 32c of Putirka (2008), uncertainty: ± 5 kbar] yields higher pressures (21.3 kbar/1308 °C, though with overlapping uncertainties) than the pressures obtained using the Jd-DiHd formulations (Table 3). Thus, the P–T of Cpx crystallization is probably ~ 15 kbar/1270 °C within ± 3.6 kbar and ± 45 °C uncertainties.

Pressures and temperatures calculated simultaneously using only the Cpx composition [4.8 kbar/1123 °C-5.4 kbar/1131 °C, with Eqs. 32a and 32d of Putirka (2008), uncertainties: ± 3.1 kbar and ± ~ 70 °C] are lower by ~ 10

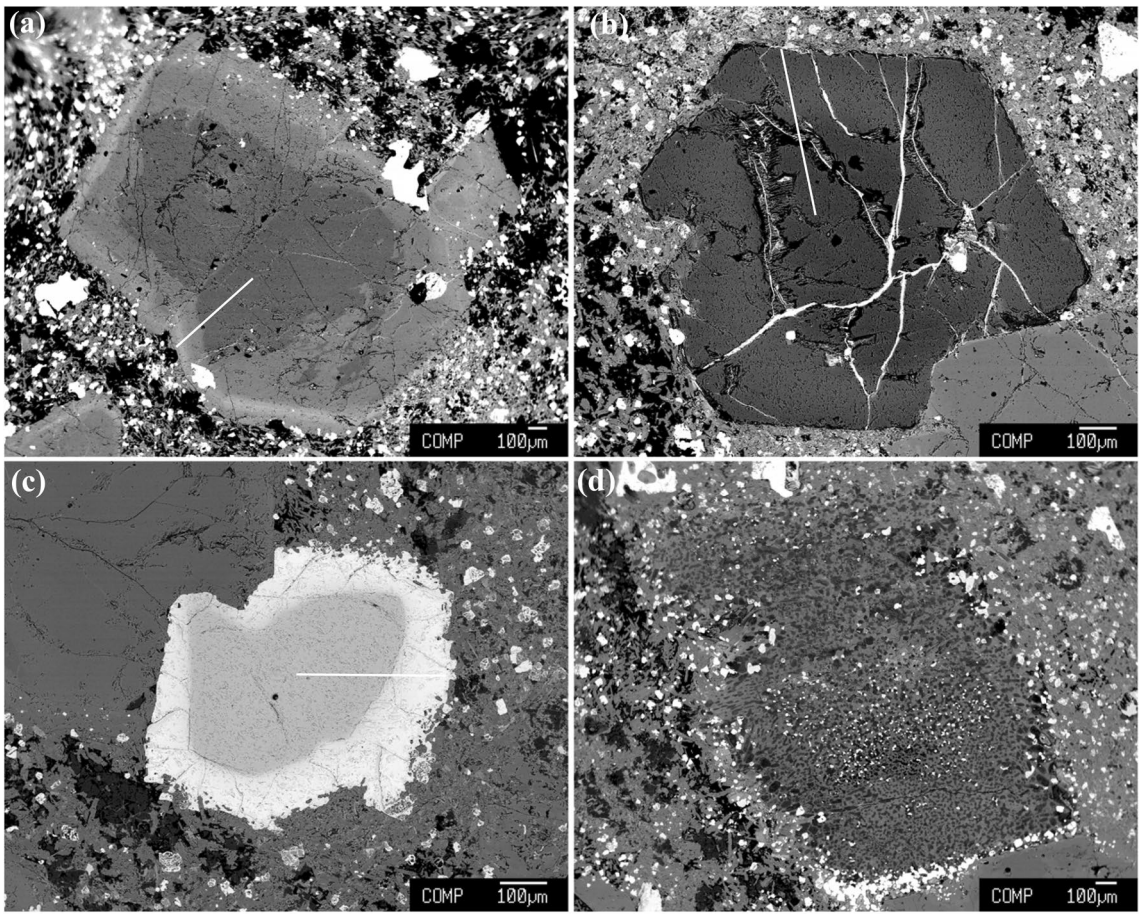

Fig. 4 BSE images showing phenocrysts of **a** clinopyroxene, **b** olivine, **c** spinel, and **d** recrystallized biotite pseudomorph surrounded by a fine-grained groundmass. Core-to-rim radial lines in (**a**–**c**) indicate the locations of compositional transects in Figs. 5 and 6

kbar and ~ 150 °C than the P–T calculated with the Cpx-liquid formulations. Equation 32a is based on the model of Nimis (1995) that recovers anomalously low pressures, e.g., the mean pressure is ~ 3 kbar lower at the experimental temperature conditions for 15 kbar experiments on a variety of compositions (Putirka 2008). In particular, simultaneous application of the Cpx-only formulations yields anomalously low P–T values for clinopyroxene (similar to Cpx in SD11, Fig. 5c, d) in equilibrium with low-SiO_2 alkalic liquids in experiments at 14–16 kbar (Holbig and Grove 2008) (lower by 6–9 kbar/80–140 °C for) and 24–33 kbar (Elkin-Tanton and Grove 2003) (lower by 7–12 kbar/70–110 °C). It appears that simultaneous P–T calculation with the Cpx-only formulations underestimates pressure by ~ 10 kbar for the Deccan alkalic rocks.

Thermobarometry of samples from previous studies

Thermobarometry was also performed on other samples using previously published data. The Sarnu melilitite sample 95-BMR-37 (Simonetti et al. 1998) shows Cpx-bulk $K_D(Fe^T–Mg)$ values of 0.28–0.30 for Cpx grains 1, 3 and 5, and the calculated P–T (13.6–15.2 kbar/1267–1284 °C) using Eqs. 30 and 33 of Putirka (2008) are similar to the calculated P–T for sample SD11 (Table 3). The lattice strain model (Blundy et al. 2020) predicts a K_D(Mn–Mg) of 0.25 at 1270 °C for olivine grain-3 (Simonetti et al. 1998) that is identical to the observed value (0.23 ± 0.08), and the calculated bulk $Fe^{3+}/\sum Fe$ ratio is 0.10. Using this $Fe^{3+}/\sum Fe$ ratio, the $K_D(Fe^{2+}–Mg)$ values for olivine-bulk (0.32) and Cpx-bulk (0.31–0.33) show equilibrium and indicate that the above P–T estimates are valid.

Two Mundwara samples (MM03 and MER06, Pande et al. 2017) show Cpx-bulk K_D ($Fe^T–Mg$) values of 0.23–0.30, and Eqs. 30 and 33 (Putirka 2008) yield P–T of 3.7–8.8 kbar/1123–1148 °C (Table 3). However, olivines in these samples with olivine-bulk $K_D(Fe^T–Mg)$ of 0.36–0.87 are probably in disequilibrium, and the bulk $Fe^{3+}/\sum Fe$ ratios were not calculated. Assuming an average bulk $Fe^{3+}/\sum Fe$ ratio of 0.13, the Cpx-bulk K_D ($Fe^{2+}–Mg$) are 0.26–0.35 indicating equilibrium, and the P–T estimates are probably valid. Pande et al. (2017) calculated similar pressures (3–7

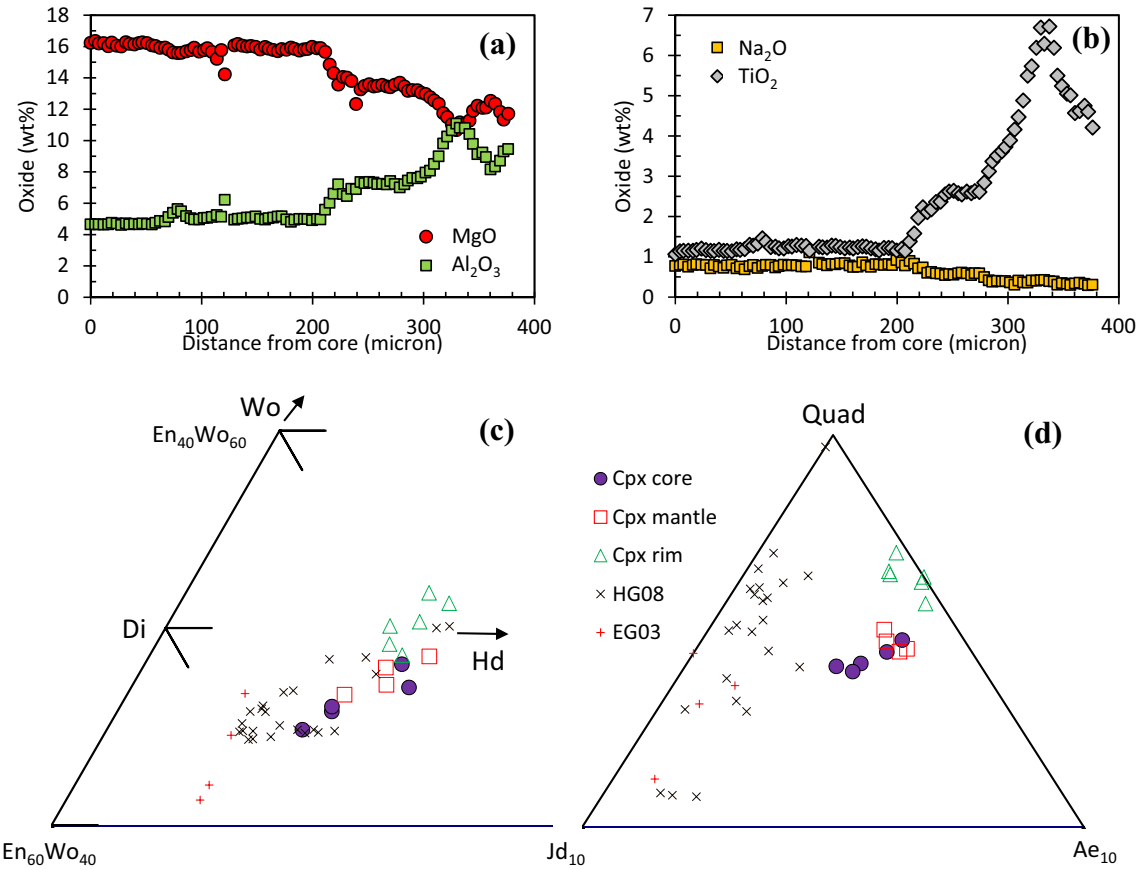

Fig. 5 **a**, **b** Core-to-rim compositional variation in clinopyroxene along transect shown in Fig. 4a. **c** Clinopyroxene compositions plotted in the enstatite (En)-diopside (Di)-hedenbergite (Hd)-ferrosilite (Fs) pyroxene quadrilateral. **d** Clinopyroxene compositions expressed as quadrilateral and non-quadrilateral (*Jd* jadeite, and *Ae* aegirine) components and plotted according to Morimoto et al. (1988). In (**c**, **d**), the data from the experiments of HB08 (Holbig and Grove 2008) and EG03 (Elkins-Tanton and Grove 2003) are shown for comparison

kbar) at 935–1030 °C for amphibole crystallization in their Mundwara samples MM11 and MM20. However, pressure obtained with the Al-exchange barometer (Eq. 32c) along with the Jd-DiHd thermometer (Eq. 33) yields higher pressures of 6.3–12.3 kbar.

The Bhuj basanite 95-BHUJ-16 (Simonetti et al. 1998) and the Murud-Janjira basanite RG3 and phonotephrite RG2 (Dessai and Viegas 2010) show high Cpx-bulk $K_D(Fe^T–Mg)$ values (0.47–0.55 and 0.44–0.48). If some Fe is considered as Fe^{3+}, the Cpx-bulk $K_D(Fe^{2+}–Mg)$ values are even higher. Hence, Cpx does not have an equilibrium Fe–Mg distribution with the bulk and the Jd-DiHd Cpx-liquid formulations are not applicable to these samples. The Cpx-only formulations (Eqs. 32a and 32d, Putirka 2008) yield pressures of 1.2–2.2 kbar that are probably ~ 10 kbar lower than the actual values (see above). Thus, these samples probably crystallized Cpx at pressures of ~ 11–12 kbar and corresponding temperatures of 1115–1156 °C (Table 3). The high pressures for the Bhuj sample are supported by results obtained with the Al-exchange barometer for Cpx-hydrous liquid that is independent of the Fe–Mg distribution. This barometer (Eq. 32c) in conjunction with the Cpx-only thermometer (Eq. 32d) yields pressures of 13.8–15.3 kbar.

Primary magmas

The primary magma compositions for primitive rocks have been traditionally determined by adding equilibrium olivine to the rock to return it to its Fo_{90}-equilibrated composition appropriate for lherzolite. Although this method works for rocks that have undergone only olivine fractionation, Till et al. (2012) demonstrated that for more evolved rocks, it is necessary to add other phases like plagioclase (Pl) and Cpx that crystallized during fractionation (e.g., Ol + Pl and Ol + Pl + Cpx). Chatterjee and Sheth (2015) calculated the primary magma compositions of Deccan tholeiites that evolved at upper crustal pressures by adding Ol + Pl + Cpx followed by Ol + Pl, and Ol only in small increments while maintaining crystal–liquid equilibrium to backtrack along their low-pressure fractionation paths until the liquids were in equilibrium with phases in lherzolite (with Fo_{90} olivine).

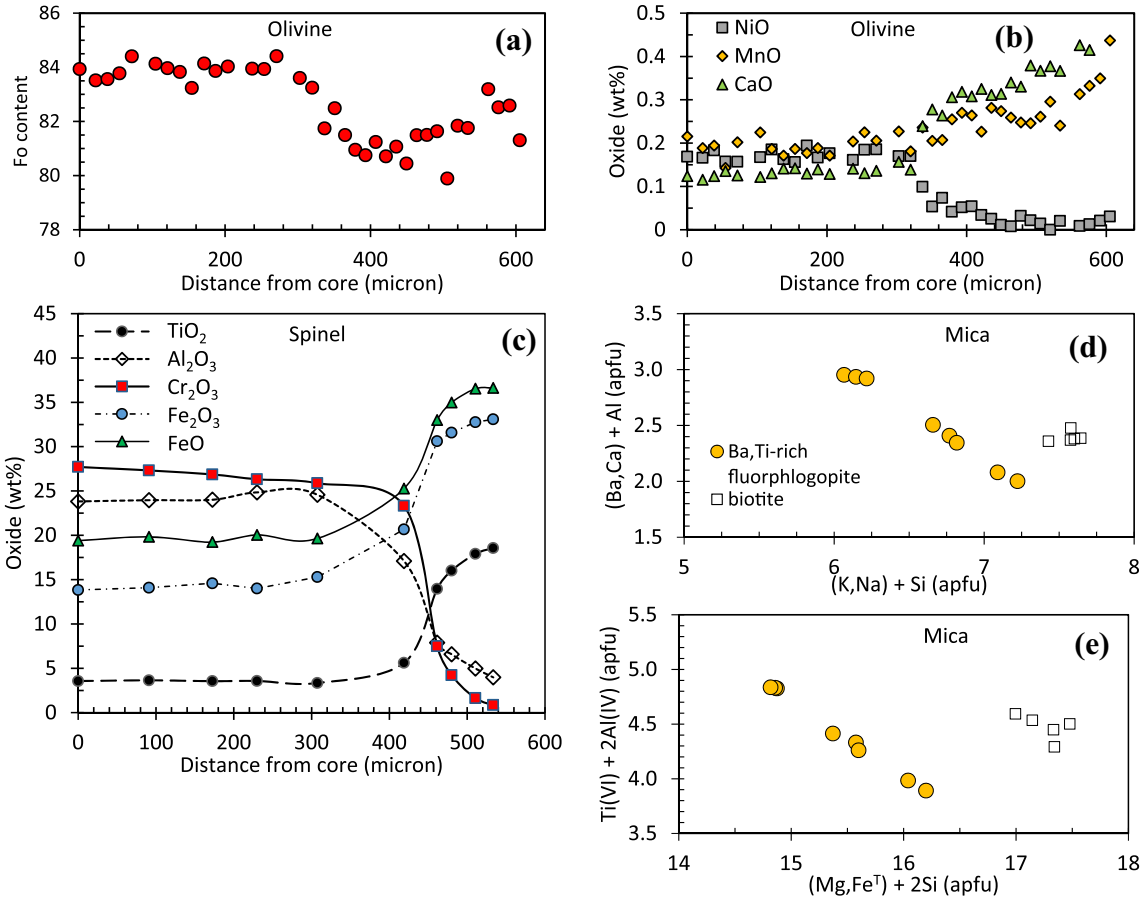

Fig. 6 **a–c** Core-to-rim compositional variation in olivine and spinel along transects shown in Fig. 4 **b–e** Compositions of mica showing incorporation of Ba and Ti by interlayer-tetrahedral and tschermak-type coupled substitutions

A similar approach was used here to calculate the primary magmas of the Deccan alkalic rocks. Thermobarometry suggests that most Deccan alkalic rocks underwent fractional crystallization at pressures of 12–15 kbar, and according to experimental constraints, primitive alkalic magmas evolve by crystallizing olivine and clinopyroxene in proportions of 11:89 at 1.4–2.2 GPa and 15:85 at 1.2 GPa between ~ 1350 and ~ 1290 °C (Holbig and Grove 2008), and 14:86 to 23:77 at 1.5 GPa and > 1200 °C (Pilet et al. 2010). The average of these proportions is Ol:Cpx = 15:85. If spinel is part of the crystallizing assemblage, as observed in the Deccan alkalic rocks, the phases crystallize in Ol:Cpx:Spl = 12:68:20 proportions (Elkins-Tanton and Grove 2003). With decreasing temperature, phlogopite joins the crystallization assemblage at ~ 1270 °C (Holbig and Grove 2008), and it is present in all Deccan alkalic rocks except the Murud-Janjira basanites. Since the Sarnu-Dandali rocks equilibrated above the temperatures of phlogopite stability (~ 1270 °C, Table 3), only Ol:Cpx:Spl = 12:68:20 phase proportions were added to calculate their primary magmas. The other Deccan rocks show equilibration temperatures of ~ 1120–1150 °C (Table 3). Hence, the primary magmas of these rocks (except Murud-Janjira basanites) were calculated by adding phases in proportions of Ol:Cpx:Spl = 12:68:20 above 1270 °C, and Ol:Cpx:Spl:Phl = 12:68:20:15 below 1270 °C (phlogopite proportion from Holbig and Grove, 2008). Amphibole is present in some Mundwara rocks and Murud-Janjira lamprophyres, but it was not considered in the calculations because it is stable at lower temperatures (< 1130 °C at 15 kbar in experiments, Pilet et al. 2010; 935–1030 °C at ~ 3–7 kbar in Mundwara rocks, Pande et al. 2017) than the equilibration temperatures of the Deccan rocks (Table 3). However, the Mundwara primary magma estimates should be treated with caution because the crystallizing-phase proportions are not well known at their 4–9 kbar pressures of equilibration.

The primary magmas of the Murud-Janjira basanites RG3 and RG1 were calculated by adding phases in Ol:Cpx:Spl = 12:68:20 proportions. In addition, the primary magmas were calculated using a reverse assimilation–fractional crystallization approach (AFC, Thompson et al. 2002) by assimilating xenoliths occurring in the lamprophyres (Dessai et al. 2004). The mass ratio of assimilated

Table 3 Thermobarometry of the Deccan alkalic rocks

Formulation	Sample	Compositions used	$K_D(Fe^T\text{-}Mg)$	$K_D(Fe^{2+}\text{-}Mg)$	P (kbar)	T (°C)	T (°C)[e]
Cpx-hydrous liquid (Jd-DiHd), Putirka (2008), P: Eq. 30 (selected data) and T: Eq. 33							
	SD11[a]	Cpx (avg), bulk	0.28	0.33	14.9	1266	
		Cpx (oc), bulk	0.29	0.34	15.5	1272	
	95-BMR-37[b]	Cpx (grain 1), bulk	0.28	0.32	13.6	1267	
		Cpx (grain 3), bulk	0.30	0.33	14.2	1272	
		Cpx (grain 5), bulk	0.28	0.31	15.2	1284	
	MM03[c]	Cpx core (grain 1), bulk	0.24	0.27	5.1	1123	
		Cpx core (grain 4), bulk	0.23	0.26	8.2	1144	
		Cpx core (grain 6), bulk	0.23	0.27	8.8	1148	
	MER06[c]	Cpx core (grain 5), bulk	0.30	0.35	4.9	1136	
		Cpx core (grain 7), bulk	0.29	0.33	3.7	1134	
Cpx-hydrous liquid (Jd-DiHd), Putirka (2008), P: Eq. 31 (global data) and T: Eq. 33							
	SD11[a]	Cpx (avg), bulk	0.28	0.33	12.2	1250	
		Cpx (oc), bulk	0.29	0.34	12.6	1255	
Cpx-anhydrous liquid (Jd-DiHd), Putirka et al. (1996), P: Eqn. P1 with T: Eqn T1							
	SD11[a]	Cpx (avg), bulk	0.28	0.33	17.0	1263	
		Cpx (oc), bulk	0.29	0.34	17.6	1267	
Cpx-hydrous liquid, Putirka (2008), P: Eq. 32c (Al exchange) and T: Eq. 33 (Jd-DiHd)							
	SD11[a]	Cpx (avg), bulk			21.3	1307	
		Cpx (oc), bulk			21.2	1308	
	95-BMR-37[b]	Cpx (grain 1), bulk			19.9	1306	
		Cpx (grain 3), bulk			22.3	1323	
		Cpx (grain 5), bulk			19.0	1309	
	MM03[c]	Cpx core (grain 1), bulk			7.9	1137	
		Cpx core (grain 4), bulk			12.3	1165	
		Cpx core (grain 6), bulk			11.1	1160	
	MER06[c]	Cpx core (grain 5), bulk			6.3	1143	
		Cpx core (grain 7), bulk			9.4	1164	
Cpx only, Putirka (2008), P: Eq. 32a and T: Eq. 32d							
	SD11[a]	Cpx (avg)			4.8	1123	1202
		Cpx (oc)			5.4	1131	1210
	95-MUN-28[b]	Cpx (grain 1)			3.3	1073	1151
		Cpx (grain 2)			3.3	1076	1153
	95-BHUJ-16[b]	Cpx (grain 1)			1.9	1043	1119
		Cpx (grain 2)			2.1	1055	1132
		Cpx (grain 3)			1.5	1054	1130
		Cpx (grain 4)			2.0	1042	1118
		Cpx (grain 5)			1.7	1063	1140
		Cpx (grain 6)			1.2	1048	1124
	RG-2[d]	Cpx core (RG2-2C)			1.8	1078	1156
	RG-3[d]	Cpx core (RG3-2C)			2.2	1039	1115
Cpx-hydrous liquid, P: Eq. 32c (Al exchange) and Cpx only, T: Eq. 32d, Putirka (2008)							
	95-BHUJ-16[b]	Cpx (grain 1)			13.8	1133	
		Cpx (grain 2)			14.4	1150	
		Cpx (grain 3)			14.9	1157	
		Cpx (grain 4)			15.3	1142	
		Cpx (grain 5)			14.5	1162	
		Cpx (grain 6)			14.6	1150	

[a]Compositions from this study

[b]Simonetti et al. (1998)

[c]Pande et al. (2017)

[d]Dessai and Viegas (2010)

[e]T recalculated with P + 10 kbar

xenoliths to fractionated crystals in each step ($r = M_a^i/M_c^i$) was fixed at 0.6, similar to olivine tholeiite fractionating at 1250 °C while assimilating tonalite at an initial temperature of 800 °C (cf. Thompson et al. 2002; the felsic granulite xenoliths show equilibration at ~ 800 °C, Dessai et al. 2004). The primary magmas of basanite were also calculated by incremental magma mixing between the primitive melts and an evolved melt represented by phonotephrite RG2 that occurs in the same intrusion as the basanites. The mixing proportions were adjusted (melt:RG2 = 55:45 for RG3, and melt:RG2 = 25:75 for RG1) until the SiO_2 contents of the primary magmas of basanite and lamprophyre were similar.

In the above calculations, average equilibrium $K_D(Fe^{2+}–Mg)$ values of 0.29 for Ol-melt, 0.28 for Cpx-melt, 0.95 for Spl-melt, and 0.21 for Phl-melt were used (Elkins-Tanton and Grove 2003; Holbig and Grove 2008), and the primary magmas (Mg# 72.3) were equilibrated with Fo_{90} olivine. Where olivine composition in the sample is known, the $Fe^{3+}/\sum Fe$ ratio of the bulk was calculated with the olivine-melt oxybarometer of Blundy et al. (2020). The lattice strain model predicts K_D(Mn–Mg) values of 0.25 for sample SD11 (olivine outer core, Fo_{81}), and 0.25 and 0.20 for samples 95-BMR-37 (olivine grain-3, Fo_{81}) and 95-BHUJ-16 (olivine grain-3, Fo_{88}, Simonetti et al. 1998) that are within the ± 0.08 uncertainties of observed K_D(Mn–Mg) values (0.32, 0.23 and 0.29), and the $Fe^{3+}/\sum Fe$ ratios of these sample are 0.16, 0.10 and 0.14, respectively. For the other samples, an average $Fe^{3+}/\sum Fe$ ratio of 0.13 was assumed. The Fe_2O_3 contents of clinopyroxene and spinel were estimated using the data in Canil and O'Neill (1996), and the $Fe^{3+}/\sum Fe$ ratio of phlogopite was assumed to be the same as that of clinopyroxene.

The uncertainties in the calculations depend on the degree of reverse fractionation required to attain the primary magma composition for each sample. For high degree of fractional crystallization, such as in sample SD11 (49%), a 10% increase in the $K_D(Fe^{2+}–Mg)$ values results in a 1.6% decrease in MgO and 3.2% increase in FeO in the primary magma (Mg# 71.3) that equilibrates with $Fo_{88.6}$ olivine. A 10% decrease in the $K_D(Fe^{2+}–Mg)$ values results in a 0.2% increase in MgO and 0.3% decrease in FeO in the primary magma Mg# (72.4) that equilibrates with $Fo_{90.1}$ olivine. Increasing the olivine proportion in the crystallizing assemblage from Ol:Cpx = 15:85 to 23:77 results in a 4.1% increase, whereas decreasing it to 11:89 results in a 2.3% decrease in both MgO and FeO. The combined uncertainties are ± 6.4% in both MgO and FeO. For Bhuj sample B (Karmalkar et al. 2005) that underwent only 2% fractional crystallization, the combined uncertainties in MgO and FeO are much lower (± 0.2%).

The calculated compositions of the Deccan alkalic primary magmas (Mg# 72.3, MgO = 12.3–16.2 wt%, Murud-Janjira basanites modeled by magma mixing) are provided in Table 4 and S4, and shown in Fig. 7. The Sarnu-Dandali primary magmas contain 38.3–39.7 wt% SiO_2, 2.0–4.3 wt% total alkali, and 14.1.16.8 wt% CaO. They mostly plot in the foidite field of the TAS diagram (Fig. 7a). The Bhuj, Mundwara and Murud-Janjira primary magmas contain higher SiO_2 (40.0–44.9 wt%), and lower CaO (10.8–14.4 wt%) and CaO/Al_2O_3, and they mostly plot in the picrobasalt and basanite (rarely in foidite) fields. The primary magmas of Murud-Janjira basanite modeled by magma mixing contain lower (1.5–2.2 wt%) TiO_2 than the other primary magmas. The Ni contents of the Deccan alkalic primary magmas are similar to the Ni contents of model peridotite-source primary magmas with ~ 12–16 wt% MgO (Herzberg et al. 2016) (Fig. 7i). Furthermore, using D_{Ni} from Beattie et al. (1991), the NiO contents of olivine (0.17–0.58 wt%) in equilibrium with the Deccan primary magmas overlap with the estimated NiO contents of olivine from primitive basalts (Mg# 89) worldwide, and experimentally derived melts of peridotite at 1–4.5 GPa (0.2–0.5 wt%, Matzen et al. 2017). The Cr contents of the Deccan alkalic primary magmas (200–1310 ppm) also overlap with the Cr content of primary melts of lherzolite (~ 750–2500 ppm, or 0.11–0.37 wt% Cr_2O_3, Liu and O'Neill 2004 and references therein). Thus, the estimated primary magma compositions in this study are consistent with the compositions of primary melts of lherzolite. The Sarnu-Dandali and Mundwara primitive alkalic rocks and the Murud-Janjira lamprophyres evolved by higher degrees (30–59%) of fractional crystallization than the Bhuj rocks (2–46%, average 26%) and the Murud-Janjira basanites (16–28%, Table S4).

Discussion

Non-lherzolitic mantle sources

Experiments on hornblendite at ~ 1.5 GPa (Pilet et al. 2008), garnet pyroxenite at 2–2.5 GPa (Hirschmann et al. 2003), and eclogite + CO_2 at 3 GPa (Dasgupta et al. 2006) have produced melts with a wide range of Mg# (36–77, assuming $Fe^{2+} = Fe^T$) that show increasing Mg# and MgO and decreasing SiO_2, TiO_2 and K_2O with the degree of melting (25–100%) (Tables 1 and 4, Fig. 2). These melts and their derivatives are comparable with the Deccan primitive alkalic rocks with similar Mg#s (51–72). The Sarnu-Dandali primitive rocks have similar MgO, total alkali, K_2O and Ce/Y, and lower SiO_2 and TiO_2 contents compared to the hornblendite melts (Fig. 2). They are lower in SiO_2 and MgO, and higher in total alkali, K_2O and TiO_2 than the pyroxenite and eclogite melts. Their CaO/Al_2O_3 ratios are higher than the hornblendite and pyroxenite melts, but lower than the eclogite melts. Primitive hornblendite, pyroxenite and

Table 4 Composition ranges of the Deccan alkalic primary magmas, experimentally derived melts and primitive rocks

	SiO_2	TiO_2	MgO	CaO	K_2O	CaO/Al_2O_3	Na_2O+K_2O	Mg#
Primary magmas								
Sarnu-Dandali	38.6–39.7	2.36–3.81	13.5–15.2	14.1–16.8	0.57–1.73	1.05–1.3	2.04–4.33	72.3
Mundwara	41–42.4	2.36–3.44	13.6–15	12.2–13.6	1.12–1.71	0.89–1.04	2.34–4.11	72.3
Bhuj	40–44.9	2.13–3.72	14–16.2	10.8–12.5	0.8–2.36	0.8–1.36	2.59–4.63	72.3
Murud-Janjira lamprophyre	41.4–42.8	2.05–2.75	14.6–15.4	11.2–12.8	1.28–1.57	0.82–1.03	2.8–3.42	72.3
Murud-Janjira basanite	43.1–44	1.21–1.83	12.3–13.6	13.8–14	0.98–1.54	1.07–1.16	3.83–5.37	72.3
Murud-Janjira basanite[a]	39.1–41.8	1.30–2.14	12.8–14.6	14.8–15.7	0.98–1.68	1.15–1.34	3.99–5.66	72.3
Murud-Janjira basanite[b]	42–42	1.45–2.12	13.8–14.6	14.3–14.4	0.8–1.64	1.2–1.25	2.79–3.96	72.3
Experimentally derived melts of non-lherzolite lithologies								
Hornblendite[c]	38.5–40.4	5.58–7.26	7.2–12.3	10.3–13.1	1.22–2.05	0.71–0.91	3.88–5.49	44.2–68.5
Cpx hornblendite[c]	41.2–44.8	3.70–5.54	9.2–12.8	12.2–17.3	0.82–1.97	0.85–1.50	2.55–5.25	57.7–74
Hornblendite/DMM[c]	44.7–46.5	3.46–5.94	9.9–13.4	9.7–11.2	0.76–1.51	0.6–0.80	2.54–4.4	67.8–74
Garnet pyroxenite[d]	42.7–45.2	1.30–2.58	10.6–15.0	9.3–11.2	0.05–0.12	0.57–0.74	1.96–3.9	59.6–74.6
Eclogite+CO_2[e]	33.8–43.3	2.60–19.40	8.2–13.5	5.1–14.7	0.02–0.20	1.46–2.10	1.88–5.3	36.3–63.6
Experimentally derived melts of lherzolite[f]								
PERC3[g]	42.4–44	1.01–1.86	15.3–16.3	14.3–17	0.02–0.11	1.18–1.7	1.25–2.78	72.4–75
PERC[g]	34.5–35.9	1.15–1.25	19.6–19.7	20.1–21.7	0.03–0.05	1.97–2.28	1.46–1.65	75.1–75.5
Lherz 0.4H 0.4C[h]	39.3–45.3	0.95–1.72	18.7–20.9	11.5–14.6	0.26–1.01	1.16–1.55	1.51–3.82	72.9–78.2
Lherz 0.7H 0.7C[h]	40.2–43.3	0.68–1.05	19.4–19.9	12.6–15.2	0.17–0.25	1.15–1.66	1.33–2.34	74.9–76.7
Rocks and experimentally derived melts of olivine leucitite[f]								
SYNWC1[i]	43.6–44.6	1.19–1.43	11.8–14.2	11.4–12.1	3–3.7	0.81–0.91	5.54–6.7	70–74.4
Oliv ugandite[j]	44.2	1.86	20.4	8.8	1.75	0.88	3.31	77
Dhandhuka[k]	47.6–48.7	2.01–2.1	13.3–15.6	11.4–13.5	0.69–0.92	1.2–1.31	2.3–2.48	68.7–71.8

Oxides in weight percent normalized to 100%, Mg# assumes $Fe^{2+}=Fe^T$ for rocks and experimentally derived melts;

[a]Calculated by reverse AFC by assimilating felsic granulite xenolith and $r = 0.6$

[b]Calculated by incremental magma mixing with phonotephrite RG2 in RG3-melt:RG2 = 55:45 and RG1-melt:RG2 = 25:75 proportions

[c]At 1.5 GPa (Pilet et al. 2008), DMM—depleted MORB mantle with hornblendite

[d]At 2–2.5 GPa (Hirschmann et al. 2003)

[e]At 3 GPa (Dasgupta et al. 2006)

[f]Only compositions with high Mg#s are shown,

[g]At 3 GPa (Dasgupta et al. 2007), PERC3 − peridotite + 1.0 wt% CO_2 and PERC − peridotite + 2.5 wt% CO_2,

[h]At 2.8 GPa (Baasner et al. 2016), 0.4H0.4C − lherzolite + 0.4 wt% H_2O+0.4 wt% CO_2 and 0.7H0.7C - lherzolite + 0.7 wt% H_2O+0.7 wt% CO_2

[i]Sierra Nevada olivine leucitite at 2.4-2.8 GPa (Elkins-Tanton and Grove 2003)

[j]Olivine ugandite (Edgar et al. 1980)

[k]Gujarat picites D6, D11 and D12 (Krishnamurthy and Cox 1977)

eclogite melts will probably evolve by clinopyroxene-dominated fractional crystallization with spinel also playing an important role. This will result in a decrease in MgO and an increase K_2O and TiO_2, whereas the trend for CaO/Al_2O_3 will depend on the clinopyroxene:spinel ratio. The CaO/Al_2O_3 ratio will decrease if clinopyroxene is the dominant crystallizing phase, but it may slightly increase if significant spinel co-crystallizes (compare with SD11, Fig. 7). Such evolutionary trends are not likely to produce melts similar to the Sarnu-Dandali primitive rocks.

The Bhuj primitive rocks have similar SiO_2, MgO, total alkali and K_2O, and lower CaO/Al_2O_3 and TiO_2 contents compared to the Cpx-hornblendite melts (Fig. 2). Fractionation of a primitive hornblendite melt will not produce melts similar to the Bhuj primitive rocks. However, the Bhuj primitive rocks are higher in CaO/Al_2O_3, K_2O and TiO_2 than the pyroxenite melts, and fractionation of a primitive pyroxenite

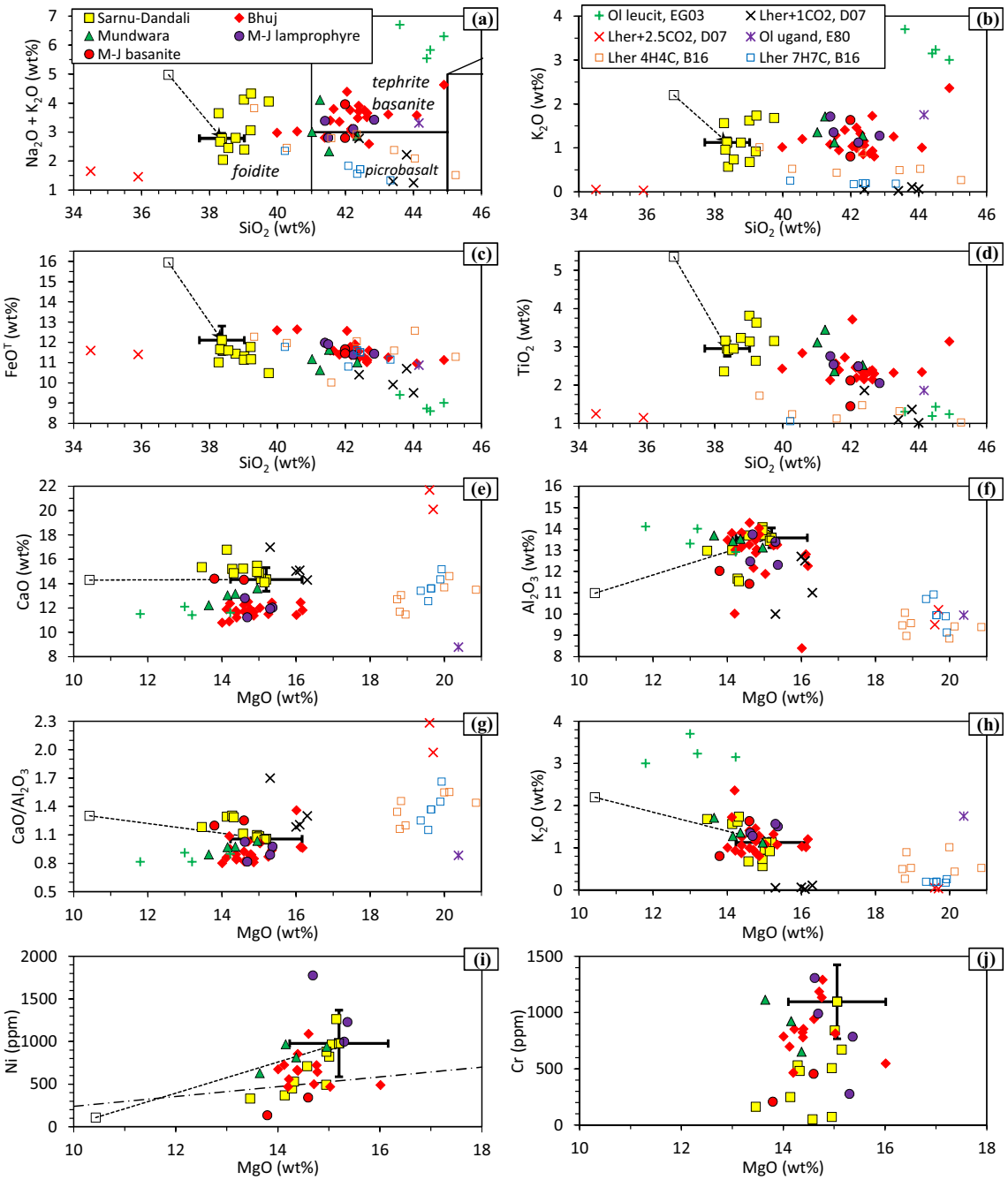

Fig. 7 Bivariate plots showing the variation of different oxides and their ratios with SiO_2 and MgO in the calculated Deccan alkalic primary magmas and experimentally generated melts and primitive rocks with Mg# 70–75 [refer to legends in (**a**, **b**)]. In (**a**), the boundaries for different rock-types are as in Fig. 2a. In (**i**), the D_{Ni} values used are 2.6 (Cpx) and 1.3 (Phl) from GERM (2021), 10.1 (Spl) from Wijbrans et al. (2015), and from the expression in Beattie et al. (1991) for olivine; the dash-dot line represents the trend for primary melts saturated with fertile lherzolite (Herzberg et al. 2016). In (**j**), the D_{Cr} values used are 1.24 (Ol), 1.66 (Cpx), 3.43 (Spl) and 5.4 (Phl) from GERM (2021). Maximum uncertainties in the primary magma estimates from uncertainties in $K_D(Fe^{2+}–Mg)$ and crystallizing-phase proportions are shown by error bars; for Ni and Cr, the error bars include uncertainties arising from the range of D_{Ni} and D_{Cr} values reported in the literature. The dashed lines with arrow connect the bulk composition of SD11 (open square) to its primary magma. The data for primitive rocks and experimentally generated melts are from EG03—Elkins-Tanton and Grove (2003), E80—Edgar et al. (1980), D07—Dasgupta et al. (2007), and B16—Baasner et al. (2016) (H_2O and CO_2 contents: 0.4 wt% in 4H4C, 0.7 wt% in 7H7C)

melt may produce melts similar to some of the Bhuj rocks. The high Ce/Y ratios of the Murud-Janjira lamprophyres and the low TiO_2 contents of the Murud-Janjira basanites (Fig. 2d, f) are not consistent with hornblendite or pyroxenite melts and their derivatives.

Whether high-Mg melts of pyroxenite can be parental to the Bhuj rocks needs to be confirmed through rigorous fractional crystallization modeling. This could not be done because Fe_2O_3 contents and proportions of phases (probably pressure-dependent) crystallizing from high-Mg melts of non-lherzolitic lithologies are not available. With the exception of some Bhuj rocks, it appears that non-lherzolitic sources for the origin of the Deccan primitive alkalic rocks are unlikely.

Lherzolitic mantle sources

High-pressure (~3 GPa) melting experiments have been performed on anhydrous and hydrous spinel- and garnet-lherzolite (Till et al. 2012; Grove et al. 2013 and references therein), garnet lherzolite with added CO_2 (Dasgupta et al. 2007, 2013) and $H_2O + CO_2$ (Baasner et al. 2016), phlogopite lherzolite (Condamine et al. 2016), and K-rich lherzolite + basalt mixtures (Davis and Hirschmann 2013). Low-degree melts produced in these experiments, and high-degree (near liquidus) melts produced in experiments on primitive basalt (Takahashi et al. 1998), hydrous basanite (Pilet et al. 2010) and olivine leucitite (Edgar et al. 1980; Elkins-Tanton and Grove 2003; Holbig and Grove 2008) are possible analogues of the calculated Deccan alkalic primary magmas in equilibrium with lherzolite.

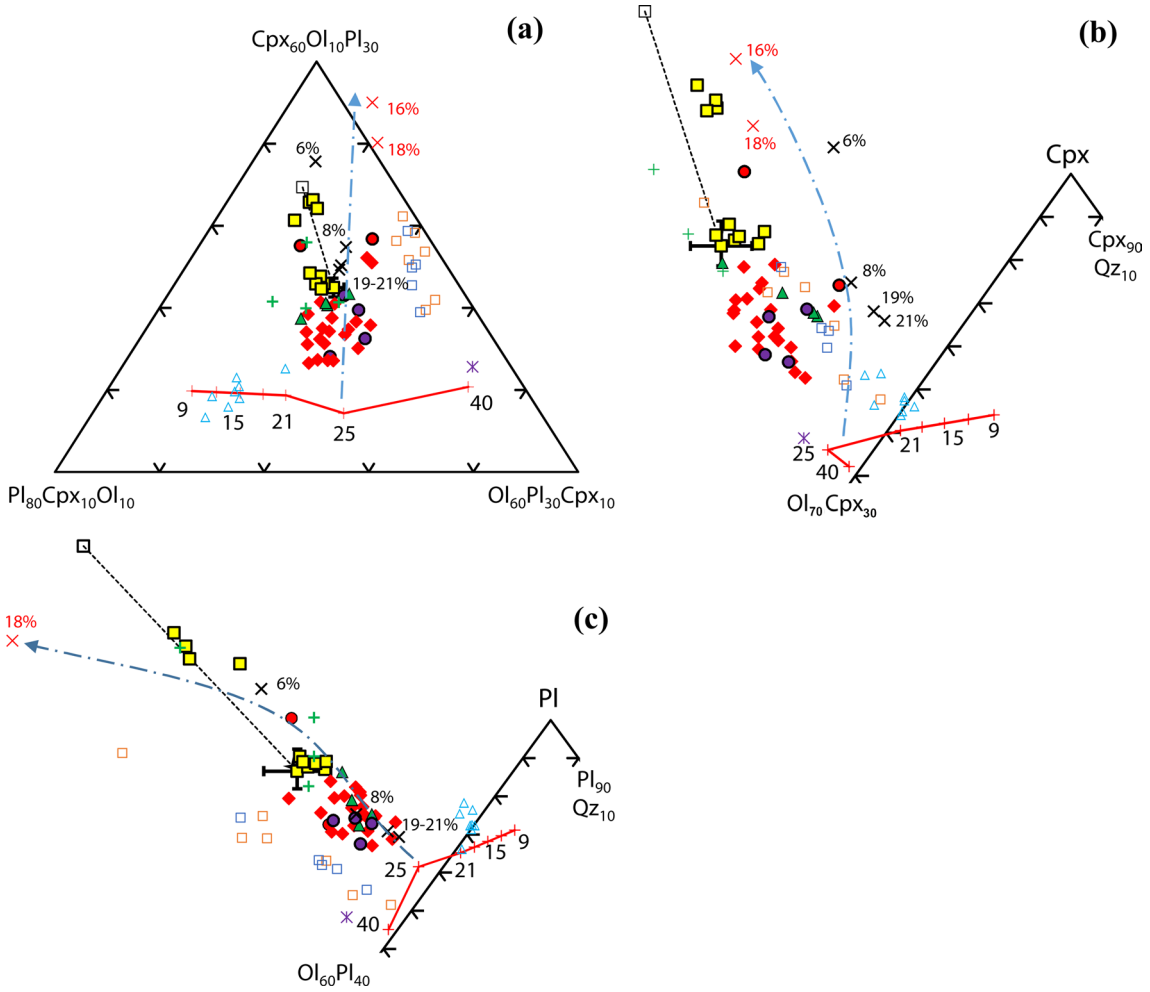

Fig. 8 Portions of the pseudoternary projections of **a** Ol-Pl-Cpx from Qz, **b** Ol-Cpx-Qz from Pl, and **c** Ol-Pl-Qz from Cpx showing the compositions of the Deccan alkalic primary magmas, experimentally derived liquids for different degrees of melting (labeled for Dasgupta et al. 2007) and primitive rocks plotted according to the scheme of Tormey et al. (1987) and Grove (1993) (symbols as in Figs. 2 and 7). Also shown are the predicted spinel lherzolite (9–21 kbar) and garnet lherzolite (25–40 kbar) multiple saturation points using the expressions of Till et al. (2012) and Grove et al. (2013) for the average Deccan alkalic primary magma on a volatile-free basis. The dot-dashed lines with arrow indicate the direction of displacement of the 25 kbar garnet lherzolite MSP with addition of CO_2 in the lherzolite source

The melts of basalt (Takahashi et al. 1998) are highly quartz normative (Grove et al. 2013) and the melts of hydrous basanite (Pilet et al. 2010) are highly enriched in Na_2O (3.5–9.4 wt%) and K_2O (1.6–3.0 wt%). These melts are very different from the Deccan primary magmas. A naturally occurring primitive olivine ugandite with Ol + Cpx + Spl + Phl on its liquidus (Edgar et al. 1980) contains similar total alkali, K_2O, FeO^T and CaO/Al_2O_3, but higher SiO_2 and MgO and lower TiO_2, CaO and Al_2O_3 than most Deccan primary magmas (Fig. 7a-h). A Sierra Nevada olivine leucitite and its near-liquidus melts in equilibrium with Ol + Cpx + Spl + Phl (Elkins-Tanton and Grove 2003) have Mg#s 70.0–74.4 (assuming $Fe^{2+} = Fe^T$) and similar CaO and Al_2O_3, but higher SiO_2, total alkali and K_2O and lower FeO^T and TiO_2 than most Deccan primary magmas (Fig. 7a-h). Thus, the high-degree melts of primitive basalt, hydrous basanite and olivine leucitite are not analogous to the Deccan primary magmas. The Deccan picrites from Dhandhuka, Gujarat, (Mg# 69–72, Krishnamurthy and Cox 1977) have many compositional similarities with the Deccan alkalic primary magmas (Table 4), but their high SiO_2 contents (47.6–48.7 wt%) imply that they are not analogous.

When the Deccan primary magmas are plotted in Ol-Pl-Cpx (from quartz, Qz), Ol-Cpx-Qz (from Pl), and Ol-Pl-Qz (from Cpx) pseudoternary projections (Fig. 8), they do not plot near their spinel- or garnet-lherzolite multiple saturation points (MSPs) predicted by the composition and pressure-dependent expressions of Till et al. (2012) and Grove et al. (2013). Compared to the Deccan primary magmas, the melts of phlogopite lherzolite (Condamine et al. 2016) and garnet lherzolite + basalt with added K_2O (Davis and Hirschmann 2013) are higher in total alkali (~ 5–11 wt%), SiO_2 (44.3–47.7 wt%) and Al_2O_3 (12.9–14.6 wt%), and the moderate-degree (16–18%) melts of lherzolite + 2.5 wt% CO_2 (Mg# 75.1–75.5, Dasgupta et al. 2007) are lower in SiO_2, total alkali, K_2O, TiO_2 and Al_2O_3 and higher in MgO and CaO (Fig. 7a-h). Thus, volatile-free lherzolite, phlogopite lherzolite, lherzolite + basalt + K_2O, and lherzolite + 2.5 wt% CO_2 are not possible sources of the Deccan alkalic primary magmas.

The 2–7% melts of lherzolite + 0.4 wt% H_2O + 0.4 wt% CO_2 (Mg# 72.9–78.2, assuming $Fe^{2+} = Fe^T$) and the 2–18% melts of lherzolite + 0.7 wt% H_2O + 0.7 wt% CO_2 (Mg# 74.9–76.7) (Baasner et al. 2016) have overlapping SiO_2, FeO^T and CaO contents and CaO/Al_2O_3 ratios with the Deccan primary magmas, but they have higher MgO and lower Al_2O_3, K_2O and TiO_2 contents (Fig. 7). The 6–21% melts of lherzolite + 1 wt% CO_2 (Mg# 72.4–75.0, Dasgupta et al. 2007) show overlapping MgO, FeO^T, Al_2O_3 and total alkali contents and CaO/Al_2O_3 ratios with the Deccan primary magmas (Fig. 7). Their SiO_2 contents are higher than the Sarnu-Dandali primary magmas, but similar to the Bhuj primary magmas. Thus, although their K_2O and TiO_2 contents are lower, they are the most similar to the Deccan primary magmas among all of the experimentally derived melts of lherzolite considered above. In the pseudoternary plots (Fig. 8), the Deccan primary magmas partially overlap with the melts from Baasner et al.'s (2016) experiments as well as the melts from experiments on lherzolite + 1 wt% CO_2 (Dasgupta et al. 2007). The melts of lherzolite + H_2O + CO_2 with higher MgO contents plot closer to the olivine apex and away from the plagioclase apex compared to the melts of lherzolite + 1 wt% CO_2. The Sarnu-Dandali primary magmas appear similar to the melts of lherzolite + 1 wt% CO_2 in the Ol–Pl–Cpx and Ol–Pl–Qz projections (Fig. 8a,c), and to the melts of lherzolite + 0.4 wt% H_2O + 0.4 wt% CO_2 in the Ol–Cpx–Qz projection (Fig. 8b). The primary magmas of the Bhuj alkalic rocks and Murud-Janjira lamprophyres are similar to the melts of lherzolite + 1 wt% CO_2 in the Ol–Pl–Qz projection (Fig. 8c). The primary magmas of the Murud-Janjira basanites are similar to the melts of lherzolite + 1 wt% CO_2 in all three projections. Thus, the Deccan alkalic primary magmas probably originated by melting of a lherzolite source containing low H_2O and CO_2 (probably < 1 wt%). A comparison of the SiO_2 and CaO contents of the Deccan primary magmas with Fig. 14 of Dasgupta et al. (2007) suggests < 0.75 wt% CO_2 in their lherzolite sources. A deep lherzolitic source is consistent with the high $^3He/^4He$ ratios of the Sarnu-Dandali and Mundwara alkalic rocks, and the REE patterns of Mundwara and Bhuj rocks have been modeled by low-degree melting of garnet lherzolite (Basu et al. 1993; Karmalkar et al. 2005).

Degree of melting

Assuming a lherzolitic source, the TiO_2 and K_2O contents of the primary magmas of Sarnu-Dandali and Bhuj primitive alkalic rocks and Murud-Janjira lamprophyres can be modeled by ~ 1–5% batch melting of a ~ 1.3 times Ti-enriched garnet lherzolite compared to primitive mantle (0.2 wt % TiO_2 and 0.029 wt % K_2O, McDonough and Sun 1995) (Fig. 9). The primary magmas of Murud-Janjira basanite contain lower (1.5–2.2 wt%) TiO_2, and they require a Ti-poor (0.7 times) garnet lherzolite source for their origin. Alternatively, the primary magmas of the Murud-Janjira lamprophyres and basanites can be modeled by batch melting of a ~ 1.7 times Ti-enriched and primitive spinel lherzolite, respectively (Fig. 9b), though garnet lherzolite is a more likely source for their origin.

Origin of the Murud-Janjira basanites

The isotopic compositions of Murud-Janjira melanephelinites and nephelinites indicate mixing between primitive mantle and a low $^{143}Nd/^{144}Nd$ lower crustal component in their source (Melluso et al. 2002). Furthermore, magma mixing

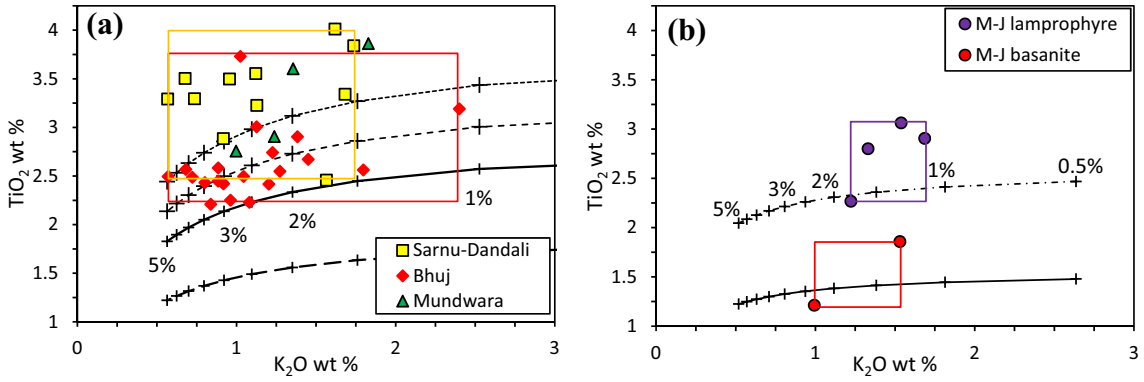

Fig. 9 The TiO_2 and K_2O contents of Deccan alkalic primary magmas (boxes show the ranges) compared with model non-modal batch melting curves for **a** primitive (solid line), Ti- poor (0.7 times, long dashed line) and Ti-enriched (1.2 times: dashed line, 1.3 times: dotted lines) garnet lherzolite with tick marks indicating melting percentages, and **b** primitive (solid line) and 1.7 times Ti-enriched (dot-dashed line) spinel lherzolite. For garnet lherzolite melting, the source contains 55% olivine, 20% Opx, 10% Cpx and 15% garnet, the melting reaction is 1 Cpx + 0.6 garnet + 0.3 olivine = 0.9 Opx + 1 liquid (Dasgupta et al. 2007), and D_{Ti} and D_K are from Davies and Hirschmann (2013). For spinel lherzolite melting, the source contains 52.5% olivine, 27% Opx, 17.5% Cpx and 3% spinel (Kinzler 1997), the melting reaction is 0.82 Cpx + 0.08 spinel + 0.4 Opx = 0.3 olivine + 1 liquid (Kinzler and Grove 1992), D_{Ti} values are from McDade et al. (2003) (olivine-melt and pyroxene-melt) and Davies et al. (2013) (spinel-melt), and D_K values are from Davies and Hirschmann (2013)

has been proposed as a mechanism for the origin of complex, reverse zoning patterns in clinopyroxene (Dessai and Viegas 2010). Hence, the compositional effects of assimilation of the lamprophyre-hosted crustal/mantle xenoliths, and mixing with evolved phonotephrite associated with the basanites (Dessai et al. 2004; Dessai and Viegas 2010) on the primary magmas of basanite are evaluated below.

The primary magmas of basanite RG1 and RG3 calculated by simple reverse fractionation show higher SiO_2, Na_2O and CaO, and lower MgO, FeO and TiO_2 than the primary magmas of lamprophyre (Fig. 10). When the primary magmas of basanite are modeled through AFC (Thompson et al. 2002) by assimilating an average felsic granulite xenolith (Dessai et al. 2004), their SiO_2 contents become lower, whereas their Na_2O and CaO contents remain high (Fig. 10). Assimilating mafic or ultramafic xenoliths results in even higher Na_2O and K_2O contents (not shown). When the primary magmas of basanite are modeled through incremental magma mixing with phonotephrite RG2 to match the SiO_2 contents of the primary magmas of lamprophyre, their Na_2O, FeO and MgO contents become similar, whereas TiO_2 remains low and CaO remains high compared to the primary magmas of lamprophyre (Fig. 10). Thus, the AFC-based model and the magma-mixing-based model generate distinctly different compositions of the primary magmas of basanite. Because RG1, RG2 and RG3 occur in the same plug, the magma mixing model for the origin of the basanites is preferred. The differences between the primary magmas of basanite modeled through magma mixing and lamprophyre may be attributed to source heterogeneities as shown above (Fig. 9).

The above modeling results suggest that the primary magmas of basanite were probably not contaminated by an AFC-type process during ascent through the Indian continental lithosphere (cf. Dessai et al. 2004). Although isotopic and some trace element evidence suggest mixing of the mantle source with a lower crustal component (Melluso et al. 1995), it is unlikely that this component was derived from the Indian lithosphere.

Melting conditions

The Deccan primary magmas ascended along adiabatic paths below the lithosphere–asthenosphere boundary (LAB), but followed the supra-solidus ~ 5% melt contour for the appropriate lherzolite composition above the LAB (Fig. 11). The approximate P–T path can be determined from the results of experiments on lherzolite + 1.0–2.5 wt% CO_2 that is 5% melted at ~ 4 GPa/1350 °C and ~ 2 GPa/1250 °C (Dasgupta et al. 2013), and lherzolite + 0.4 wt% H_2O + 0.4 wt% CO_2 that is ~ 4% melted at ~ 2.8 GPa/1345 °C (Baasner et al. 2016). The 5% melt contour appropriate for the lherzolite source of the Deccan primary magmas (thin red line, Fig. 11) is probably located approximately between the melt contours inferred from the above two studies. Geophysical studies constrain the depths of the LAB at 85–90 km (~ 2.7 GPa) below Sarnu-Dandali (Radha Krishna et al. 2002), 63–69 km (~ 1.9 GPa) below Bhuj (Mandal and Pandey 2011), and ~ 40 km (~ 1.3 GPa) below Murud-Janjira (Negi et al. 1992). At these depths, the temperatures at the top of the melting column were approximately 1325 °C, 1290 °C,

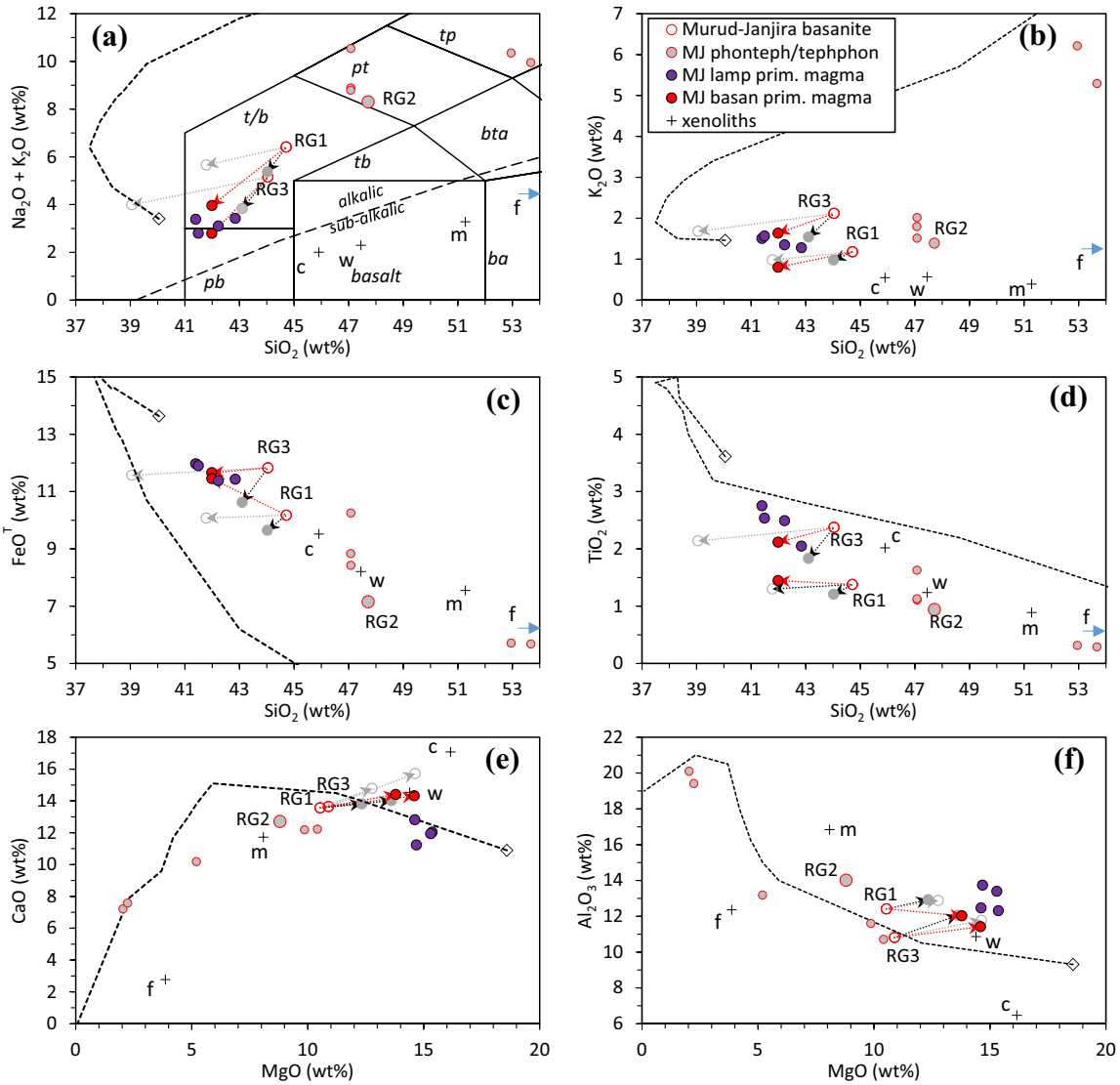

Fig. 10 Bivariate plots showing model primary magmas of Murud-Janjira basanites RG1 and RG3 calculated through reverse fractionation (filled grey circles), reverse AFC by assimilating felsic granulite (open grey circles), and incremental magma mixing with phonotephrite RG2 (filled red circles). Basanites, phonotephrites and tephriphonolites (Melluso et al. 2002; Dessai and Viegas 2010), average xenoliths (Dessai et al. 2004), and the primary magmas of lamprophyre are also shown. The dotted lines represent model trends for the evolution of Cape Verde lavas from a primary melt (diamond) (Weidendorfer et al. 2016). The abbreviations are: *pb* picrobasalt, *t/b* tephrite/basanite, *pt* phonotephrite, *tp* tephriphonolite, *tb* trachybasalt, *bta* basaltic trachyandesite, *ba* basaltic andesite, *c* clinopyroxenite, *w* websterite, *m* mafic granulite, and *f* felsic granulite with 69.8 wt% SiO_2 (plots outside the figure areas in **a**–**d**)

and 1280 °C beneath Sarnu-Dandali, Bhuj, and Murud-Janjira, respectively.

Conclusion

The Deccan primitive alkalic rocks mostly crystallized at high pressures beneath the Moho with clinopyroxene equilibrating at ~ 15 kbar/1270 °C at Sarnu-Dandali and at ~ 11–12 kbar/1115–1156 °C at Bhuj and Murud-Janjira. Their primary magma compositions (Mg# 72.3, MgO = 12.3–16.2 wt%) in equilibrium with Fo_{90} olivine were calculated by incrementally adding equilibrium phases in Ol:Cpx:Spl:Phl = 12:68:20:15 proportions at low temperatures and Ol:Cpx:Spl = 12:68:20 proportions at higher temperatures (only the latter proportions were used for the Sarnu-Dandali rocks that equilibrated at high temperatures and the Murud-Janjira basanites that lack phlogopite). The Sarnu-Dandali and Mundwara primitive alkalic rocks and the Murud-Janjira lamprophyres require higher degrees (30–59%) of reverse fractional crystallization than the Bhuj rocks (2–46%) and the Murud-Janjira basanites (16–28%) to

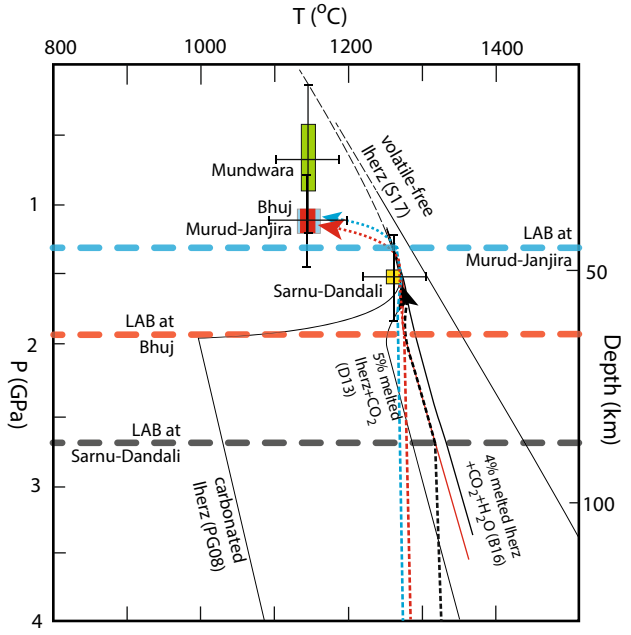

Fig. 11 Approximate mantle melting conditions for the Deccan alkalic rocks. The volatile-free (S17—Sarafian et al. 2017) and CO_2-saturated (PG08—Presnall and Gudfinnsson 2008) peridotite solidi are shown for reference. The melt contours in black are for ~ 5% melted lherzolite + 1.0–2.5 wt% CO_2 (D13—Dasgupta et al. 2013) and ~ 4% melted lherzolite + 0.4 wt% CO_2 + 0.4 wt% H_2O (B16—Baasner et al. 2016), and in red for the approximately ~ 5% melted lherzolite source of the Deccan alkalic rocks. The thick dashed lines represent geophysically constrained lithosphere-asthenophere boundaries (LAB) beneath Sarnu-Dandali (black), Bhuj (red) and Murud-Janjira (blue). The colored boxes with error bars indicate the P–T of crystallization for the Deccan alkalic rocks determined through thermobarometry. The dotted lines with arrow indicate the approximate P–T paths followed by the Sarnu-Dandali (black), Bhuj (red) and Murud-Janjira (blue) magmas

achieve equilibration with lherzolite. In a total alkali-silica diagram, the modeled Sarnu-Dandali primary magmas plot in the foidite field, and the modeled Bhuj, Mundwara and Murud-Janjira primary magmas mostly plot in the picrobasalt and basanite fields.

With the exception of some Bhuj rocks, non-lherzolitic sources are unlikely for the Deccan alkalic rocks. The modeled Deccan alkalic primary magmas show Ni and Cr contents consistent with melts of lherzolite, and their major element compositions show similarities to melts derived in ~ 3 GPa experiments on lherzolite + 1 wt% CO_2 (Dasgupta et al. 2007) and lherzolite + 0.4–0.7 wt% H_2O + 0.4–0.7 wt% CO_2 (Baasner et al. 2016). Hence, they probably originated by melting of lherzolite containing low (< 1 wt%) H_2O and CO_2. The TiO_2 and K_2O contents of the primary magmas of the Sarnu-Dandali and Bhuj alkalic rocks and Murud-Janjira lamprophyres can be explained by < 5% melting of a ~ 1.3 times Ti-enriched garnet lherzolite source compared to primitive mantle. Reverse AFC modeling by assimilating lower crustal and mantle xenoliths suggests that the primary magmas of Muruj-Janjira basanites were not contaminated by the Indian continental lithosphere during ascent. Magma mixing with evolved melts was more important in their origin. Their primary magmas contain lower (1.5–2.2 wt%) TiO_2 than the other Deccan alkalic primary magmas, and they likely originated by melting of a Ti-poor (0.7 times) garnet lherzolite source. The experimental constraints on lherzolite melting (Dasgupta et al. 2007; Baasner et al. 2016) and geophysical constraints on the depth of the lithosphere–asthenosphere boundary indicate that the approximate temperatures at the top of the melting column were ~ 1325 °C beneath Sarnu-Dandali, and ~ 1285 °C beneath Bhuj, and Murud-Janjira.

Supplementary Information The online version contains supplementary material available at https://doi.org/10.1007/s00410-021-01787-4.

Acknowledgements I am grateful to Etienne Médard and two anonymous reviewers for their critical and extremely constructive reviews that greatly improved the presentation of this manuscript. Comments from the editor, Othmar Müntener, discussions with Tim Grove, and minor comments from Stephanie Krein are also greatly appreciated. I thank Jon Blundy for sharing his olivine oxybarometer spreadsheet that was very helpful in the calculations. The Sarnu-Dandali sample SD11 was kindly provided by Hetu Sheth.

References

Armstrong JT (1995) CITZAF—a package for correction programs for the quantitative electron microbeam x-ray analysis of thick polished materials, thin-films and particles. Microbeam Anal 4:177–200

Baasner A, Médard E, Laporte D, Hoffer G (2016) Partial melting of garnet lherzolite with water and carbon dioxide at 3 GPa using a new melt extraction technique: implications for intraplate magmatism. Contrib Mineral Pet 171:45

Basu AR, Renne PR, Das Gupta DK, Teichmann F, Poreda RJ (1993) Early and late alkali pulses and a high ^{3}He plume origin for the Deccan flood basalts. Science 261:902–906

Beane JE, Turner CA, Hooper PR, Subbarao KV, Walsh JN (1986) Stratigraphy, composition and form of the Deccan basalts, Western Ghats, India. Bull Volcanol 48:61–83

Beattie P, Ford C, Russell D (1991) Partition coefficients for olivine-melt and orthopyroxene-melt systems. Contrib Mineral Pet 109:212–224

Bhattacharji S, Chatterjee N, Wampler JM, Nayak PN, Deshmukh SS (1996) Indian intraplate and continental margin rifting, lithospheric extension and mantle upwelling in Deccan flood basalt volcanism near K/T boundary: evidence from mafic dike swarms. J Geol 104:379–398

Blundy J, Melekhova E, Ziberna L, Humphreys MCS, Cerantola V, Brooker RA, McCammon CA, Pichavant M, Ulmer P (2020) Effect of redox on Fe–Mg–Mn exchange between olivine and melt and an oxybarometer for basalts. Contrib Mineral Pet 175:103

Bose MK (1973) Petrology and geochemistry of the igneous complex of Mount Girnar, Gujarat, India. Contrib Mineral Pet 39:247–296

Canil D, O'Neill HSC (1996) Distribution of ferric iron in some upper-mantle assemblages. J Pet 37(3):609–635

Campbell IH, Griffiths RW (1990) Implications of mantle plume structure for the evolution of flood basalts. Earth Planet Sci Lett 99:79–93

Chandrasekaran V, Srivastava RK, Chawade MP (1990) Geochemistry of the alkalic rocks of Sarnu-Dandali area, District Barmer, Rajasthan, India. J Geol Soc India 36:365–382

Chatterjee N, Sheth H (2015) Origin of the Powai ankaramite, and the composition, P-T conditions of equilibration and evolution of the primary magmas of the Deccan tholeiites. Contrib Mineral Pet 169:32

Condamine P, Médard E, Devidal J-L (2016) Experimental melting of phlogopite-peridotite in the garnet stability field. Contrib Mineral Petrol 171:95

Courtillot V, Gallet Y, Rocchia R, Féraud G, Robin E, Hofmann C, Bhandari N, Ghevariya ZG (2000) Cosmic markers, $^{40}Ar/^{39}Ar$ dating and paleomagnetism of the KT sections in the Anjar area of the Deccan large igneous province. Earth Planet Sci Lett 182:137–156

Dasgupta R, Hirschmann MM, Stalker K (2006) Immiscible transition from carbonate-rich to silicate-rich melts in the 3 GPa melting interval of eclogite + CO_2 and genesis of silica-undersaturated ocean island lavas. J Pet 47:647–671

Dasgupta R, Hirschmann MM, Smith ND (2007) Partial melting experiments of peridotite +CO_2 at 3 GPa and genesis of alkalic ocean island basalts. J Pet 48:2093–2124

Dasgupta R, Mallik A, Tsuno K, Withers AC, Hirth G, Hirschmann MM (2013) Carbon-dioxide-rich silicate melt in the Earth's upper mantle. Nature 493:211–215

Davis F, Hirschmann M (2013) The effects of K_2O on the compositions of near-solidus melts of garnet peridotite at 3 GPa and the origin of basalts from enriched mantle. Contrib Mineral Pet 166(4):1029–1046

Davis FA, Humayun M, Hirschmann MM, Cooper RS (2013) Experimentally determined mineral/melt partitioning of first-row transition elements (FRTE) during partial melting of peridotite at 3 GPa. Geochim Cosmochim Acta 104:232–260

Dessai AG, Viegas A (2010) Petrogenesis of alkaline rocks from Murud-Janjira in the Deccan Traps, Western India. Mineral Pet 98:297–311

Dessai AG, Rock NMS, Griffin BJ, Gupta D (1990) Mineralogy and petrology of some xenolth bearing alkaline dykes associated with Deccan magmatism, south of Bombay, India. Eur J Min 2:667–685

Dessai AG, Marckwick A, Vaselli O, Downes H (2004) Granulite and pyroxenite xenoliths from the Deccan Trap: insight into the nature and composition of the lower lithosphere beneath cratonic India. Lithos 78:263–290

Devey CW, Lightfoot PC (1986) Volcanological and tectonic control of stratigraphy and structure in the western Deccan Traps. Bull Volcanol 48:195–207

Edgar AD, Condliffe E, Barnett RL, Shirran GJ (1980) An experimental study of an olivine ugandite magma and mechanisms for the formation of its K-enriched derivatives. J Pet 21:475–497

Elkins-Tanton LT, Grove TL (2003) Evidence for deep melting of hydrous metasomatized mantle: Pliocene high-potassium magmas from the Sierra Nevadas. J Geophys Res 108(B7):2350

Gast PW (1968) Trace element fractionation and origin of tholeiitic and alkaline magma types. Geochim Cosmochim Acta 32:1057–1086

GERM (2021) Geochemical earth reference model partition coefficient (Kd) database. Earth Ref. org. https://earthref.org/KDD/. Accessed Jan 2021

Green DH (1973) Conditions of melting of basanite magma from garnet peridotite. Earth Planet Sci Lett 17:456–465

Grove TL (1993) Corrections to expressions for calculating mineral components in "Origin of calc-alkaline series lavas at Medicine Lake volcano by fractionation, assimilation and mixing" and "Experimental petrology of normal MORB near the Kane Fracture Zone: 22°–25°N, mid-Atlantic ridge." Contrib Mineral Pet 114:422–424

Grove TL, Holbig ES, Barr JA, Till CB, Krawczynski MJ (2013) Melts of garnet lherzolite: experiments, models and comparison to melts of pyroxenite and carbonated lherzolite. Contrib Mineral Pet 166:887–910

Herzberg C, Vidito C, Starkey NA (2016) Nickel-cobalt contents of olivine record origins of mantle peridotite and related rocks. Am Mineral 101:1952–1966

Hirschmann MM, Kogiso T, Baker MB, Stolper EM (2003) Alkalic magmas generated by partial melting of garnet pyroxenite. Geology 31:481–484

Holbig ES, Grove TL (2008) Mantle melting beneath the Tibetan Plateau: experimental constraints on the generation of ultrapotassic lavas from Qiangtang. Tibet J Geophys Res 113:B04210

Karmalkar NR, Rege S, Griffin WL, O'Reilly SY (2005) Alkaline magmatism from Kutch, NW India: implications for plume-lithosphere interaction. Lithos 81:101–119

Kinzler RJ (1997) Melting of mantle peridotite at pressures approaching the spinel to garnet transition: application to mid-ocean ridge basalt petrogenesis. J Geophys Res 102:853–874

Kinzler RJ, Grove TL (1992) Primary magmas of mid-ocean ridge basalts.1. Exp Methods J Geophys Res 97:6885–6906

Kogiso T, Hirschmann MM, Frost DJ (2003) High-pressure partial melting of garnet pyroxenite: possible mafic lithologies in the source of ocean island basalts. Earth Planet Sci Lett 216:603–617

Krishnamurthy P, Cox KG (1977) Picrite basalts and related lavas from the Deccan Traps of western India. Contrib Mineral Pet 62:53–75

Krishnamurthy P, Pande K, Gopalan K, Macdougall JD (1999) Mineralogical and chemical studies on alkaline basaltic rocks of Kutch, Gujarat, India. Mem Geol Soc India 43:757–783

Kshirsagar PV, Sheth HC, Shaikh B (2011) Mafic alkali magmatism in central Kachchh, India: amonogenetic volcanic field in the northwestern Deccan Traps. Bull Volcanol 73:595–612

Le Bas MJ, Le Maitre RW, Streckeisen A, Zanettin B (1986) A chemical classification of volcanic rocks based on the total alkali-silica diagram. J Petrol 27:745–750

Lightfoot PC, Hawkesworth CJ, Devey CW, Rogers NW, van Calsteren PWC (1990) Source and differentiation of Deccan Trap lavas: implications of geochemical and mineral chemical variations. J Pet 31:1165–1200

Liu X, O'Neill HSC (2004) The Effect of Cr_2O_3 on the partial melting of spinel lherzolite in the system CaO–MgO–Al_2O_3–SiO_2–Cr_2O_3 at 1·1 GPa. J Pet 45(11):2261–2286

Macdonald GA, Katsura T (1964) Chemical composition of Hawaiian lavas. J Pet 5:82–133

Mandal P, Pandey OP (2011) Seismogenesis of the lower crustal intraplate earthquakes occurring in Kachchh, Gujarat, India. J Asian Earth Sci 42:479–491

Matzen AK, Wood BJ, Baker MB, Stolper EM (2017) The roles of pyroxenite and peridotite in the mantle sources of oceanic basalts. Nat Geosci 10:530–535

McDade P, Blundy JD, Wood BJ (2003) Trace element partitioning on the Tinaquillo Lherzolite solidus at 1.5 GPa. Phys Earth Planet Inter 139:129–147

McDonough WF, Sun S-s (1995) The composition of the Earth. Chem Geol 120:223–253

McKenzie D, Bickle MJ (1988) The volume and composition of melt generated by extension of the lithosphere. J Petrol 29:623–679

Melluso L, Beccaluva L, Brotzu P, Gregnanin A, Gupta AK, Morbidelli L, Traversa G (1995) Constraints on the mantle sources of the Deccan Traps from the petrology and geochemistry of basalts of Gujarat state, western India. J Pet 36:1393–1432

Melluso L, Sethna SF, D'Antonio M, Javeri P, Bennio L (2002) Geochemistry and petrogenesis of soidic and potassic mafic alkaline rocks in the Deccan Volcanic Province, Mumbai area (India). Mineral Pet 74:323–342

Mitchell C, Widdowson M (1991) A geological map of the southern Deccan Traps, Indian and its structural implications. J Geol Soc Lond 148:495–505

Morgan WJ (1972) Deep mantle convection plumes and plate tectonics. Bull Am Assoc Petrol Geol 56:203–213

Morimoto N, Fabries J, Ferguson AK, Ginzburg IV, Ross M, Seifert FA, Zussman L, Aoki K, Gottardi G (1988) Nomenclature of pyroxenes. Mineral Mag 52:535–550

Negi JG, Agrawal PK, Singh AP, Pandey OP (1992) Bombay gravity high and eruption of Deccan flood basalts (India) from a shallow secondary plume. Tectonophys 206:341–350

Nimis P (1995) A clinopyroxene geobarometer for basaltic systems based on crystals-structure modeling. Contrib Mineral Pet 121:115–125

Pande K, Cucciniello C, Sheth H, Vijayan A, Sharma KK, Purohit R, Jagadeesan KC, Shinde S (2017) Polychronous (early cretaceous to palaeogene) emplacement of the Mundwara alkalic complex, Rajasthan, India: $^{40}Ar/^{39}Ar$ geochronology, petrochemistry and geodynamics. Intern J Earth Sci 106:1487–1504

Paul DK, Ray A, Das B, Patil SK, Biswas SK (2008) Petrology, geochemistry and paleomagnetism of the earliest magmatic rocks of Deccan Volcanic Province, Kutch, Northwest India. Lithos 102:237–259

Pertermann M, Hirschmann MM, Hametner K, Gunther D, Schmidt MW (2004) Experimental determination of trace element partitioning between garnet and silica-rich liquid during anhydrous partial melting of MORB-like eclogite. Geochem Geophys Geosyst. https://doi.org/10.1029/2003GC000638

Pilet S, Baker MB, Stolper EM (2008) Metasomatized lithosphere and the origin of alkaline lavas. Science 320:916–919

Pilet S, Ulmer P, Villiger S (2010) Liquid line of descent of a basanitic liquid at 1.5 GPa: constraints on the formation of metasomatic veins. Contrib Mineral Pet 159:621–643

Presnall DC, Gudfinnsson GH (2008) Origin of the oceanic lithosphere. J Petrol 49:615–632

Putirka KD (2008) Thermometers and barometers for volcanic systems. Rev Mineral Geochem 69:61–120

Putirka K, Johnson M, Kinzler R, Walker D (1996) Thermobarometry of mafic igneous rocks based on clinopyroxene-liquid equilibria, 0–30 kbar. Contrib Mineral Pet 123:92–108

Radha Krishna M, Verma RK, Purushotham AK (2002) Lithospheric structure below the eastern Arabian Sea and adjoining West Coast of India based on integrated analysis of gravity and seismic data. Marine Geophys Res 23:25–42

Rao KM, Ravi Kumar M, Rastogi BK (2015) Crust beneath the northwestern Deccan Volcanic Province, India: evidence for uplift and magmatic underplating. J Geophys Res Solid Earth 120:3385–3405

Richards MA, Duncan RA, Courtillot VE (1989) Flood basalts and hotspot tracks: plume heads and tails. Science 246:103–107

Roeder PL, Emslie RF (1970) Olivine liquid equilibrium. Contrib Mineral Pet 29:275–289

Sano T, Fujii T, Deshmukh SS, Fukuoka T, Aramaki S (2001) Differentiation processes of Deccan Trap basalts: contribution from geochemistry and experimental petrology. J Pet 42:2175–2195

Sarafian E, Gaetani GA, Hauri EH, Sarafian AR (2017) Experimental constraints on the damp peridotite solidus and oceanic mantle potential temperature. Science 355(6328):942–945

Schoene B, Eddy MP, Samperton KM, Keller CB, Keller G, Adatte T, Khadri SFR (2019) U-Pb constraints on pulsed eruption of the Deccan Traps across the end-Cretaceous mass extinction. Science 363:862–866

Sen G, Bizimis M, Das R, Paul DK, Ray A, Biswas S (2009) Deccan plume, lithosphere rifting, and volcanism in Kutch, India. Earth Planet Sci Lett 277:101–111

Sheth H, Pande K, Vijayan A, Sharma KK, Cucciniello C (2017) Recurrent early cretaceous, indo-madagascar (89–86 Ma) and deccan (66 Ma) alkalic magmatism in the Sarnu-Dandali complex, Rajasthan: $^{40}Ar/^{39}Ar$ age evidence and geodynamic significance. Lithos 284–285:512–524

Simonetti A, Goldstein SL, Schmidberger SS, Viladkar SG (1998) Geochemical and Nd, Pb, and Sr isotope data from Deccan alkalic complexes: inferences for mantle sources and plume-lithosphere interaction. J Pet 39:1847–1864

Sprain CJ, Renne PR, Vanderkluysen L, Pande K, Self S, Mittal T (2019) The eruptive tempo of Deccan volcanism in relation to the Cretaceous-Paleogene boundary. Science 363:866–870

Takahashi E, Nakajima K, Wright TL (1998) Origin of the Columbia Rivers basalts: melting model of a heterogeneous plume head. Earth Planet Sci Lett 162:63–80

Thompson AB, Matile L, Ulmer P (2002) Some thermal constraints on crustal assimilation during fractionation of hydrous, mantle-derived magmas with examples from central Alpine batholiths. J Petrol 43:403–422

Till CB, Grove TL, Krawczynski MJ (2012) A melting model for variably depleted and enriched lherzolite in the plagioclase and spinel stability fields. J Geophys Res 117:B06206

Tischendorf G, Forster H-J, Gottesmann B, Rieder M (2007) True and brittle micas: composition and solid-solution series. Mineral Mag 71:285–320

Tormey DR, Grove TL, Bryan WB (1987) Experimental petrology of normal MORB near the Kane Fracture Zone: 22–25°N, mid-Atlantic Ridge. Contrib Mineral Pet 96:121–139

Vijayan A, Sheth H, Sharma KK (2016) Tectonic significance of dykes in the Sarnu-Dandali alkalic complex, Rajasthan, northwestern Deccan Traps. Geosci Front 7:783–791

Wadia DN (1975) Geology of India, 4th edn. Tata McGraw-Hill, p 508

Weidendorfer D, Schmidt MW, Mattsson HB (2016) Fractional crystallization of Si-undersaturated alkaline magmas leading to unmixing of carbonatites on Brava Island (Cape Verde) and a general model of carbonatite genesis in alkaline magma suites. Contrib Mineral Pet 171:43

Wijbrans CH, Klemme S, Berndt J, Vollmer C (2015) Experimental determination of trace element partition coefficients between spinel and silicate melt: the influence of chemical composition and oxygen fugacity. Contrib Mineral Pet 169:45